NASA Technical Memorandum 108853

User's Guide for ENSAERO–A Multidisciplinary Program for Fluid/Structural/Control Interaction Studies of Aircraft (Release 1)

Guru P. Guruswamy, Ames Research Center, Moffett Field, California

October 1994

National Aeronautics and Space Administration

Ames Research Center
Moffett Field, California 94035-1000

User's Guide for ENSAERO–A Multidisciplinary Program for Fluid/Structural/Control Interaction Studies of Aircraft (Release 1)

Guru P. Guruswamy

Ames Research Center

Summary

Strong interactions can occur between the flow about an aerospace vehicle and its structural components resulting in several important aeroelastic phenomena. These aeroelastic phenomena can significantly influence the performance of the vehicle. At present, closed-form solutions are available for aeroelastic computations when flows are in either the linear subsonic or supersonic range. However, for aeroelasticity involving complex nonlinear flows with shock waves, vortices, flow separations, and aerodynamic heating, computational methods are still under development. These complex aeroelastic interactions can be dangerous and limit the performance of aircraft. Examples of these detrimental effects are aircraft with highly swept wings experiencing vortex-induced aeroelastic oscillations, transonic regime at which the flutter speed is low, aerothermoelastic loads that play a critical role in the design of high-speed vehicles, and flow separations that often lead to buffeting with undesirable structural oscillations. The simulation of these complex aeroelastic phenomena requires an integrated analysis of fluids and structures. This report presents a summary of the development, applications, and procedures to use the multidisciplinary computer code ENSAERO. This code is based on the Euler/Navier–Stokes flow equations and modal/finite-element structural equations.

Introduction

Understanding the nature of flows and their interactions with structures is becoming increasingly important for aerospace vehicles. High performance and maneuverability are playing major roles in design. Flows over modern aircraft such as High Speed Civil Transport (HSCT) and Advanced Subsonic Civil Transport (ASCT) are quite often complex, and are associated with vortices and shock waves. Formation of vortices changes the aerodynamic load distribution on a wing. Vortices formed on aircraft have caused several instabilities such as aeroelastic oscillations for a highly swept flexible wing (refs. 1 and 2). In the transonic regime, aircraft experience low flutter speeds due to moving shock waves (refs. 3 and 4). Such instabilities can severely impair the performance of an aircraft. On the other hand, there are possibilities of using the vortices to control aircraft at high angles of attack when some of the conventional control techniques are not adequate. Advanced methods such as active controls, are being developed to control the aircraft aeroelastic oscillations. Strong interactions between fluids and structures occur through the control surfacess (refs. 5 and 6). In addition, thermal loads can further complicate such interactions for high-speed vehicles such as hypersonic aircraft (ref. 7).

For accurate computation of flows and including interactions with structures, it is necessary to solve the Navier–Stokes equations and couple them with the structural equations. Recently, methods were developed to accurately couple the Euler (ref. 8) and Navier–Stokes (ref. 9) solutions with the structural equations and they are incorporated in a multidisciplinary aeroelastic code, ENSAERO. This new code computes aeroelastic responses by simultaneously integrating the Euler/Navier–Stokes equations and the structural equations of motion using aeroelastically adaptive dynamic grids. The flow is solved by time-accurate finite difference schemes based on the Beam-Warming algorithm (refs. 10 and 11). The code was used to make computations for flexible wings to demonstrate the effects of vortical flows (ref. 9).

In this report, the development and applications of the multidisciplinary code ENSAERO is presented. This work is a part of a larger effort within the Computational Aerosciences Branch of Ames Research Center to further develop efficient multidisciplinary codes to compute flows over aerospace vehicles, including thermal loads and active controls. The flow equations are based on the Euler/Navier–Stokes equations. This new code is being designed in a modular fashion to adapt several different numerical schemes suitable for accurate aeroelastic computations. The candidate flow solvers are based on schemes such as central difference schemes with artificial viscosity (ref. 11), the streamwise upwind schemes (ref. 12), etc. The basic coding accommodates patched zonal grid techniques for efficient modeling of full aircraft (ref. 13). This computational capability is also being designed in such a way that finite elements can be directly used for more complete modeling of structures. This will be an improvement over the modal approach that is currently used. Several multidisciplinary modules such as active controls, thermoelastic displacements, etc., are also implemented.

This report describes the procedure of coupling the flow solutions with the structural equations of motion, including active controls and thermal loads. Results are demonstrated for steady/unsteady flow computations on rigid full aircraft configurations and aeroelastic responses of wings/wing-body configurations. A detailed user's manual is also given to run the code on current vector supercomputers such as Cray C-90.

The author thanks Dr. Chansup Byun and Dr. Shigeru Obayashi of MCAT institute in preparing this guide. He also appreciates the feedback received from several users of the code from industries and universities.

Governing Aerodynamics Equations

The strong conservation law form of the Navier–Stokes equations is used for shock-capturing purposes. The equations in Cartesian coordinates in nondimensional form can be written as

$$\frac{\partial Q}{\partial t}+\frac{\partial E}{\partial x}+\frac{\partial F}{\partial y}+\frac{\partial G}{\partial z}=\frac{\partial E_\nu}{\partial x}+\frac{\partial F_\nu}{\partial y}+\frac{\partial G_\nu}{\partial z} \quad (1)$$

To enhance numerical accuracy and efficiency and to handle boundary conditions more easily, the governing equations are transformed from the Cartesian coordinates to general curvilinear coordinates where

$$\begin{aligned} \tau &= t \\ \xi &= \xi(x,y,z,t) \\ \eta &= \eta(x,y,z,t) \\ \zeta &= \zeta(x,y,z,t) \end{aligned} \quad (2)$$

The resulting transformed equations are not much more complicated than the original Cartesian set and can be written in nondimensional form as

$$\frac{\partial}{\partial \tau}\hat{Q}+\frac{\partial}{\partial \xi}(\hat{E}-\hat{E}_v)+\frac{\partial}{\partial \eta}(\hat{F}-\hat{F}_v)+\frac{\partial}{\partial \zeta}(\hat{G}-\hat{G}_v)=0 \quad (3)$$

where $\hat{}$ indicate the transformed quantities.

In order to solve equation 3 for the full flow, a very fine grid throughout the flow field is required. In high Reynolds number flows, the viscous effects are confined to a thin layer near rigid boundaries. In most practical cases, because of computer storage and speed limitations, there are only enough grid points to resolve the gradients normal to the body by clustering the grid in the normal direction, and resolution along the body is similar to what is needed in inviscid flow calculations. As a result, even though the full derivatives are retained in the equations, the gradients along the body are not resolved unless the streamwise and circumferential grid spacings are sufficiently small. Hence, for many Navier–Stokes computations, the viscous derivatives along the body are dropped. This leads to the thin-layer Navier–Stokes equations. In this paper the thin-layer Navier–Stokes form of equation 3 is used for modeling the flow.

The thin-layer model requires a boundary-layer type coordinate system. In our case, the ξ and η directions are along the body and the viscous derivatives associated with these directions are dropped, whereas the terms in ζ are retained and the body surface is mapped onto a constant ζ surface. Thus, equation 3 simplifies to

$$\partial_\tau \hat{Q}+\partial_\xi \hat{E}+\partial_\eta \hat{F}+\partial_\zeta \hat{G}=Re^{-1}\partial_\zeta \hat{S} \quad (4)$$

It should be emphasized that the thin-layer approximation is valid only for high Reynolds number flows. Also, very large turbulent eddy viscosities invalidate the model.

Aerodynamics Solution Procedures

Computational efficiency is a major requirement in selecting solution procedures. In multidisciplinary computations, the solution of aerodynamic equations requires about 50% of the computational time. As a result, numerical efficiency of the aerodynamic solution procedure is an important factor in multidisciplinary code development.

Several numerical schemes have been developed to solve equation 4. To date, one of the well tested schemes is the implicit approximate factorization algorithm of Beam and Warming (ref. 10) based on central differencing. The diagonal implicit form of the Beam-Warming method reported by Pulliam and Chaussee (ref. 11) further reduces the computational time. The central difference scheme requires specification of an artificial dissipation to stabilize the computations. Often such artificial dissipations lead to dissipative solutions. In order to overcome this deficiency of central difference schemes, upwind schemes were developed. To date most of the upwind schemes are based on flux-splitting in the coordinate direction. Recently, Obayashi and Goorjian (ref. 12) have developed a new upwind scheme based on flux-splitting in the streamwise direction. This new streamwise upwind scheme computes flows more accurately than the coordinate-direction upwind schemes.

The current version of ENSAERO has both options of central differencing and streamwise upwinding. Both methods are equally efficient in computational speed.

One of the main bottlenecks in using the Navier–Stokes equations is the lack of proper turbulence modeling. Solving turbulent flows directly without modeling the turbulence is a very difficult task because of the extreme time and space scales associated with turbulent motion. Hence, to date the most common method of simulating turbulent flows is through an approximate turbulence model that is implemented into the Reynolds-averaged Navier–Stokes equations. In this work the turbulence model proposed by Baldwin-Lomax (ref. 14) is used.

Aeroelastic Equations of Motion

The governing aeroelastic equations of motion of a flexible wing are solved using the Rayleigh-Ritz method. In this method, the resulting aeroelastic displacements at any time are expressed as a function of a finite set of assumed modes. The contribution of each assumed mode to the total motion is derived by Lagrange's equation. Furthermore, it is assumed that the deformation of the continuous wing structure can be represented by deflections at a set of discrete points. This assumption facilitates the use of discrete structural data, such as the modal vector, the modal stiffness matrix, and the modal mass matrix. These can be generated from a finite-element analysis or from experimental influence-coefficient measurements. In this study, the finite-element method is used to obtain the modal data.

It is assumed that the deformed shape of the wing can be represented by a set of discrete displacements at selected nodes. From the modal analysis, the displacement vector $\{d\}$ can be expressed as

$$\{d\} = [\phi]\{q\} \tag{5}$$

where $[\phi]$ is the modal matrix and $\{q\}$ is the generalized displacement vector.

The final matrix form of the aeroelastic equations of motion is

$$[M]\{\ddot{q}\} + [G]\{\dot{q}\} + [K]\{q\} = \{F\} \tag{6}$$

where [M], [G], and [K] are modal mass, damping, and stiffness matrices, respectively. $\{F\}$ is the aerodynamic force vector defined as $(\frac{1}{2})\rho U_{\infty}^2[\phi]^T[A]\{\Delta C_p\}$ and $[A]$ is the diagonal area matrix of the aerodynamic control points.

The aeroelastic equation of motion, equation 6, is solved by a numerical integration technique based on the linear acceleration method (ref. 15).

Finite-element Structures

The use of finite elements is a well developed technology for solving structural problems. General-purpose codes based on finite element methods, such as NASTRAN, are available for analyzing structures coupled with linear aerodynamics. On the other hand, to solve the nonlinear flow problems, finite-element methods are still in their early stages of development when compared to finite-difference methods. For ENSAERO, finite differences for flows and finite elements for structures are used. Coupling between the two methods is achieved by interpolation. Modes generated by a shell/plate element available in the code are shown in figure 1.

One of the purposes of this work is to conduct aerothermoelastic analysis of aerospace vehicles such as NASP. The finite elements used in the present development can model the thermal loads. It is assumed that the temperature distribution is given by the aerodynamic equations. To treat thermal loads, the analysis method is divided into two steps. First, assuming that all nodal points are restrained, the stresses developed within all elements due to temperature changes are found. Next the element corner forces that maintain these stresses are obtained. Then to eliminate these corner forces the system is analyzed for nodal point loads which are equal in magnitude but opposite in sign to these restraining forces. These nodal forces are added to the aerodynamic loads. More details can be found in books such as reference 16. A procedure of modeling the thermal loads in a finite-element program is illustrated by this author in chapter 13 of reference 16.

An equation similar to equation 6 can be solved using the direct matrices from the finite element method in place of the modal matrices. The thermal loads can be added to the right hand side of equation 6. Thermal stress capability is available as a special option in the code.

Active Control Surfaces

Many physically important phenomena occur in engineering because of strong coupled interactions between structures and fluids. One such case is the use of wings with control surfaces. Aerodynamic means can be developed through active controls to counter the forces and moments that drive flutter and dynamic instability. Use of active control is important for future aircraft which will tend to be more complex for high maneuverability.

In the past, a procedure for simulating the active coupling of structures and nonlinear flows was presented (ref. 5) using transonic small disturbance equations. The approach was oriented towards synthesizing active controls of aeroelastically oscillating wings with unsteady transonics in the time domain. This procedure was implemented in the TSP (transonic small perturbation) code ATRAN3S (ref. 5) and the role of shock waves on active controls was studied. The scheme presented in ATRAN3S work is general in nature and can be extended to study engineering problems where structures and fluids are strongly coupled through some type of active control system.

The present work, a procedure similar to the one available in ATRAN3S is implemented in ENSAERO. It is assumed that a control law is known from detailed control theory analysis for a given configuration. By using the present procedure the coupled phenomena of structures, aerodynamics, and active controls can be accurately simulated. A typical control law in the time domain can be assumed as

$$\delta = G_1 h_1(t) e^{i\psi_1} + G_2 \alpha_1(t) e^{i\psi_2} \tag{7}$$

where

δ	control surface deflection
G_1, G_2	gain factors
h_1	deflection at a selected point on the wing
α_1	angle of attack at a selected span station
ψ_1, ψ_2	phase angles

By representing the active control law in the above form, the coupled phenomena of structures, aerodynamics, and active controls can be studied in a realistic time domain.

One major difference between ATRAN3S and ENSAERO is in grids. Grids are not moved in ATRAN3S for control surfaces because of the use of the small disturbance equations. Since ENSAERO uses Euler/Navier–Stokes equations, grids need to be moved according to the control surface movements. Currently, control surface deflections are modeled by shearing the grid which is valid for moderate control surface angles-of-attack up to about 6 deg. A complete method which uses a sliding zonal grid is also available in a special version of the code.

Configuration-adaptive Moving Grids

One of the major problems in computational aerodynamics using the Euler/ Navier–Stokes equations lies in the area of grid generation. For the case of steady flows, advanced techniques such as zonal grids (ref. 13) are being used for full aircraft. Such a grid-generation technique for aeroelastic calculations involving moving components is developed for ENSAERO (ref. 17). The effects of the aeroelastic-configuration-adaptive dynamic grids on the stability and accuracy of the numerical schemes are being studied in detail.

In this work, the zonal grid technology based on the work in reference 13 is implemented. Figure 2 illustrates a schematic approach to go from zonal grids in the physical space to the computational space. Figure 3 illustrates the overlapping of a fine grid with a coarse grid for a two-zone grid. In the current development this procedure is extended to moving grids (ref. 17).

An important part of this dynamic grid system was the development of an algebraic grid-generation technique for aeroelastic applications. The algebraic method was selected to minimize the computational overhead caused by grid generation. For accurate aeroelastic computations, grids need to be generated at each time step. Such analytical methods as those based on solving the elliptic differential equations are computationally expensive.

The grid scheme in ENSAERO satisfies four general requirements for a successful grid, namely: 1) the grid lines intersect normal to the wing surface in the chordwise direction, 2) the grid cells are smoothly stretched away from the wing surface, 3) the outer boundaries are located far from the wing to minimize the effect of boundary reflections, and 4) the grids adapt to the deformed wing position at each time step.

For wings the code generates both surface and field grids. The input is required in the form of standard engineering data such as surface coordinates in user defined Cartesian grid system. The field grids used for wings in this study have a C-H topology, as shown in figure 4 for a typical blended wing-body configuration. The grid deforms to remain coincident with the wing surface as it deflects, while the outer boundary of the grid is fixed in space. At the end of each time step, the deformed shape of the wing is computed using equation 5 including the control surface deflections given by equation 7. The ξ and η grid distributions on the grid surface corresponding to the wing surface (ζ grid index = 1) are obtained from previously assumed distributions. These distributions are selected to satisfy the general requirements of a grid for accurate computations. In this work, the grid in the ξ direction is selected so that the grid spacing is small near the wing and stretches exponentially to the outer boundaries. The grid near the leading edge is made finer than the rest of the wing in order to model the geometry accurately. In the spanwise direction, a uniformly distributed grid spacing is used on the wing. To model the wing tip, a finer grid spacing is used. Away from the wing tip, the η grid spacing stretches exponentially. The ζ grid spacing is computed at each time step using the deformed shape of the wing computed using equation 5. The ζ grid lines start normal to the surface in the chordwise direction and their spacing stretches exponentially to a fixed outer boundary. To prevent the outer boundaries from moving, the grid is sheared in the ζ direction. The metrics required in the computational domain are computed using the following relations

$$\begin{aligned}
\xi_t &= -x_\tau \xi_x - y_\tau \xi_y - z_\tau \xi_z \\
\eta_t &= -x_\tau \eta_x - y_\tau \eta_y - z_\tau \eta_z \\
\zeta_t &= -x_\tau \zeta_x - y_\tau \zeta_y - z_\tau \zeta_z
\end{aligned} \tag{8}$$

The grid velocities x_τ, y_τ, and z_τ required in equation 8 are computed using the grids at new and old time levels. This adaptive grid-generation scheme is incorporated into ENSAERO. The ability of this scheme to compute accurate aeroelastic responses has been demonstrated in reference 8.

Grid capability similar to wings is also available for wing-body configurations. However, for a wing-body configuration the surface flow solver grid is required as an input. The H-O type field grid is generated by the code. Figure 5 shows the deformed grid generated by the code for a typical wing-body configuration.

Currently the code assumes that only the grids in the zones attached to the surface are allowed to move. The grid movements approach zero near the zonal outer boundaries that interface with other zones. This assumption minimizes errors caused by the moving zonal interfaces. General approaches where zonal interfaces can move relative to one another is also available in special versions of the code described later in this report.

Computational efficiency and robustness of the solution method are important for CPU time intensive aeroelastic calculations with configuration-adaptive grids. Therefore, a numerically efficient diagonal algorithm is used. The diagonal algorithm computes time-accurate calculations in a geometrically nonconservative fashion. Geometric conservation can improve the accuracy of the results for moving grids. However, studies have shown that satisfying geometric conservation has little effect on the solutions associated with moving grids. The time steps used for Navier–Stokes calculations are typically small enough that the error from geometric nonconservation is negligible for most practical purposes.

The validation of computed results with experiments reported in this paper and in reference 17 further supports the use of the diagonal scheme for computations associated with moving grids. In order to maintain the efficiency and robustness of the diagonal scheme, the present time-accurate computations are made in a geometrically nonconservative fashion.

Code Design

Computational methods and computer hardware are continually evolving and growing technologies. Modular coding procedures and hardware independence can minimize software maintenance cost, particularly for multidisciplinary codes. NASTRAN, one of the successful codes of NASA for structural analysis is a typical example of highly modular coding. Similar efforts have been made for codes based on CFD. ATRAN3S of NASA Ames Research Center (ref. 5) is a hardware-independent code written in modular fashion which has been successfully used for multidisciplinary research involving fluids/structures/active controls. However, several issues, such as grids, were simple in ATRAN3S because of the use of the small disturbance equations.

ENSAERO is being designed as a multidisciplinary code. For portability it is written in standard FORTRAN-77. It contains eight main modules, namely: 1) input processor, 2) grid generation, 3) flow solver, 4) finite elements structures, 5) aeroelastic solution, 6) active controls, 7) thermal loads, and 8) post processor. Each module is independent of others for the purposes of code development and adding new features. Most of the communication among modules take place through COMMON BLOCK data. An automated bookkeeping utility, NUPDATE, that is available on most of the super computers such as Cray Y-MP, Cray C-90, etc., is utilized in programming. This kind of typical computerized bookkeeping technique is highly suitable for the multiprogrammer environment of writing large scientific codes. Such an environment is essential for multidisciplinary code development since several analysts and programmers from different disciplines need to mutually coordinate. A special version of the code is also maintained by less versatile but more easily available UNIX utility "make." A flow diagram of the code is illustrated in figure 6.

Currently the code is being developed on Cray computers at Ames Research Center, Numerical Aerodynamic Simulation (NAS) Systems Division. The current version of ENSAERO runs at 400 million floating point operations per second (MFLOPS) on a single processor of Cray C-90 computer. The central processing unit (CPU) time per time step per grid point is 5×10^{-6} sec, and the memory required per grid point is about 30 words with the use of a secondary storage. The memory required per grid point can be further reduced by using the zonal grids in the code. Details of input options for version 2.3 that has built-in grids for wings with moving control surfaces and modal structures is given in appendix A. A sample input is given in appendix B.

Illustrations

In this section, some results from ENSAERO to illustrate its various capabilities are shown. Most of the multidisciplinary results illustrate the coupling between flow and structures. Computations are made using both central difference and upwind options of the code. Unless stated all results are presented for turbulent flows.

Steady Pressures

The steady-state option of the present development is same as the TNS code capability with zonal grids. (ref. 13) Currently, for steady state computation the code can model full aircraft such as the F-16. Figure 7 illustrates the steady pressure contours on the F-16 aircraft by using 27 zones. The capability of the code to compute separated flows is already demonstrated (ref. 13). The capability of the code to compute flows at moderate to high angles of attack is illustrated in figure 8 by computing the lifts up to 20 deg angle of attack for a delta wing.

Unsteady Pressures on Rigid Configurations in Oscillating Motion

ENSAERO has an option of computing unsteady flows over wings in oscillating and ramp motions. In the code, an efficient procedure is provided to switch between Euler and Navier–Stokes equations. Figure 9 shows the Euler and Navier–Stokes unsteady pressures on the AGARD rectangular wing in a pitching motion taken from reference 17. The wing is pitching about the mid-chord with a reduced frequency k based on a root chord equal to 0.27. The Navier–Stokes results compare better with the experiment than do the Euler results.

The present code has an important capability of zonal grids which was earlier developed for the steady state computations. This zonal grid capability is extended for moving grids (ref. 17). Figure 10 illustrates the two-zone computation on the AGARD rectangular wing in pitching motion. The smooth variation of Mach contours through the zonal interface can be seen in the figure. This illustrates the potential of the present code to treat complete geometry with moving zonal grids.

The geometry capability in the code can handle general wing motions. This is illustrated by computing the unsteady pressures over the F-5 wing oscillating in a pitching mode as shown in figure 11. The unsteady pressures at subsonic Mach number are shown in figure 12. More details can be found in reference 12.

Unsteady Pressures on Rigid Configurations in Ramp Motion

In this section, ENSAERO is demonstrated to compute flow over a typical wing-body configuration shown in figure 9 pitching from α = 0.0 to 15.0 deg in a ramp motion. All computations for the rigid configuration at M_∞ = 0.90 and Re_c = 1.52 × 10^6, using a time-step size of 2 × 10^{-3}. From numerical experiments, it was found that the time-step size used is adequate to obtain a stable and accurate unsteady solution.

Computations were made at two pitch rates (A) 0.10 and 0.050. The pitch rate, A, is defined as $\dot{\alpha}c/U_\infty$ where α is in radians. Figure 13 shows computed responses of lift, moment, and drag for both pitch rates. Both computed and measured steady state results are also shown for comparison. The comparison is reasonable except for some discrepancies near peaks of lift and moment coefficient curves. In general, lifts and moments compare better than drag with the experiment. More details about these calculations and also for wing-body-canard configuration can be found in references 18 and 19, respectively.

Aeroelastic Computations

As stated in the introduction, one of the unique features of ENSAERO is the ability to accurately compute aeroelastic responses associated with vortical/transonic/separated flows which are highly nonlinear in nature. Significant details of physics may be lost if the flow details are neglected. To illustrate the importance of the flow on aeroelasticity, results are demonstrated for a flexible blended wing-body configuration. The mode shapes and frequencies of the first six modes computed using the finite-element method are shown in figure 14. This configuration experienced AOA (angle of attack) dependent aeroelastic oscillations associated with vortical flows. Figure 15 shows the presence of a strong vortex on the wing for 10.5 deg AOA. Figure 16 shows the aeroelastic responses at 0, 8, and 12 deg AOA. As it was observed in the wind tunnel measurements (ref. 1), the configuration experiences a sustained aeroelastic oscillations at 8 deg AOA due to interaction between a strong vortex and wing flexibility. At 0 deg AOA, aeroelastic oscillations are not observed since there is no vortex on the wing. At 12 deg AOA, again no oscillations are observed due weakening of vortex from flow separation. More details are given in reference 9. Other current multidisciplinary codes such as NASTRAN, ATRAN3S/XTRAN3S, etc. that use low fidelity flow equations cannot predict this phenomenon.

Moving Control Surfaces

The present development can be used for computing aeroelastic responses of aircraft with active controls. The code has the capability to model moving control surfaces by using sliding and sheared grids (ref. 19). Figure 17 illustrates the comparison of unsteady pressures with the experiment for a wing with oscillating control surface. Figure 18 shows snapshots of unsteady pressures for full wing-body configuration with antisymmetric oscillations of control surfaces. More details can be found in references 20 and 21.

Special Options in the Code

Continuous effort is being made to enhance the capability of the ENSAERO code. One of the major efforts is to incorporate full finite element structures capability. References 22 and 23 describe the implementation of wing-box and shell/plate finite element capabilities into the code. Another major effort is to develop a parallel version of the code. A wing-body version has been successfully implemented on Intel's iPSC/860 computer. References 24 and 25 describe the details about parallel implementation. Recently an LU-SGS flow solver combined with pseudo-dynamic aeroelastic solver option was added to the code to considerably reduce CPU time for static aeroelastic computations (ref. 26). Robust general mismatch sliding boundary interface capability is also available as described in reference 27. Other special options such as Johnson-King turbulence model, structural thermal stress capability etc. are also available with the code.

Conclusions

In this report, the computational code ENSAERO developed for multidisciplinary computations involving fluid/structural interactions is described. The code uses a moving patched zonal grid concept to model complex flexible aerospace vehicles. The flow is modeled using the Euler/Navier–Stokes equations, and computations are made using efficient methods based on both central and upwind schemes. The structure is represented by both modal and finite-element equations to model general aerospace vehicles. Provisions are made to accommodate other disciplines such as controls. The capability of the code to compute unsteady flows on flexible configurations with transonic/vortical flows is demonstrated. The present development is a useful computational tool for the multidisciplinary area involving fluid/structural/control interactions. Parallel implementation of this computational tool on the state-of-the-art parallel computers such as Intel iPSC 860 has successfully begun.

References

1. Dobbs, S. K.; Miller, G. D.; and Stevenson, J. R.: Self Induced Oscillation Wind Tunnel Test of a Variable Sweep Wing. AIAA Paper 85-0739-CP, 1985.

2. Guruswamy, G. P.; Goorjian, P. M.; Ide, H.; and Miller, G. D.: Transonic Aeroelastic Analysis of the B-1 Wing. J. Aircraft, **23**, 547–553, 1986.

3. Farmer, M. G.; and Hanson, P. W.: Comparison of Supercritical and Conventional Wing Flutter Characteristics. NASA TM-X-72837, 1976.

4. Ashley, H.: Role of Shocks in the Sub-transonic Flutter Phenomenon. J. Aircraft, **17**, 187–197, 1980.

5. Guruswamy, G. P.: Integrated Approach for Active Coupling of Structures and Fluids. AIAA J., **27**, 788–793, 1989.

6. Guruswamy, G. P.; and Tu, E. L.: Transonic Aeroelasticity of Fighter Wings with Active Control Surfaces. J. Aircraft, **26**, 682–684, 1989.

7. Edwards, T. A.; and Flores, J.: Towards a CFD Nose-to-Tail Capability: Hypersonic Unsteady Navier–Stokes Code Validation. AIAA Paper 89-1672, 1989.

8. Guruswamy, G. P.: Unsteady Aerodynamics and Aeroelastic Calculations for Wings Using Euler Equations. AIAA J., **28**, 461–469, 1990.

9. Guruswamy, G. P: Vortical Flow Computations on Swept Flexible Wings Using Navier–Stokes Equations. AIAA J., vol. 28, no. 12, Dec. 1990, pp. 2077–2133.

10. Beam, R.; and Warming, R. F.: An Implicit Finite Difference Algorithm for Hyperbolic Systems in Conservation-law Form. J. Comp. Phys., **22**, 87–110, 1976.

11. Pulliam, T. H.; and Chaussee, D. S.: A Diagonal Form of an Implicit Approximate Factorization Algorithm. J Comp. Phys., **39**, 347–363, 1981.

12. Obayashi, S.; Guruswamy, G. P.; and Goorjian, P. M.: Streamwise Upwind Algorithm for Computing Unsteady Transonic Flows Past Oscillating Wings. AIAA J., vol. 29, no. 10, October 1991, pp. 1668–1677.

13. Flores, J.: Simulation of Transonic Viscous Wing and Wing-Fuselage Flows using Zonal Methods. NASA TM-89421, 1987.

14. Baldwin, B. S.; and Lomax, H.: Thin Layer Approximation and Algebraic Model for Separated Turbulent Flows. AIAA Paper 78-257, 1978.

15. Guruswamy, G. P.; and Yang, T. Y.: Aeroelastic Time Response Analysis of Thin Airfoils by Transonic Code LTRAN2. Computers and Fluids, **9**, 409–425, 1980.

16. Yang, T. Y.: Finite Element Structural Analysis, Prentice Hall, New York, 1986.

17. Chaderjian, N.; and Guruswamy, G. P.: Unsteady Transonic Navier–Stokes Computations for an Oscillating Wing using Single and Multiple zones. AIAA Paper 90-0313, 1990.

18. Obayashi, S.; Guruswamy, G. P.; and Tu, E. L.: Unsteady Navier–Stokes Computations on a Wing-Body Configuration in Ramp Motions. AIAA Paper 91-2865-CP, August 1991.

19. Obayashi, S.; and Guruswamy, G. P.: Navier–Stokes Computations for Oscillating Control Surfaces. AIAA Paper 92-4431, August 1992.

20. Tu, E.; Obayashi, S.; and Guruswamy, G. P.: Unsteady Navier–Stokes Simulation of the Canard-Wing-Body-Configuration. AIAA Paper 93-3058, July 1993.

21. Obayashi, S.; Chiu, I.; and Guruswamy, G. P.: Navier–Stokes Computations on Full-Span Wing-Body Configuration with Oscillating Control Surfaces. AIAA Paper 93-3687, August 1993.

22. MacMurdy, D.; Guruswamy, G. P.; and Kapania, R.: Aeroelastic Analysis of Wings Using Euler/Navier–Stokes Equations Coupled with Improved Wing-Box Finite Element Structures. AIAA Paper 94-1587, April 1994.

23. Guruswamy, G. P.; and Byun, C.: Fluid-Structural Interactions Using Navier–Stokes Flow Equations with Shell Finite-element Structures. AIAA Paper 93-3087, July 1993.

24. Byun, C.; and Guruswamy, G. P.: A Comparative Study of Serial and Parallel Aeroelastic Computations. NASA TM-108805, Jan. 1994.

25. Byun, C.; and Guruswamy, G. P.: Wing-Body Aeroelasticity Using Finite-Difference Fluid/Finite-Element Structural Equations on Parallel Computers. AIAA Paper 94-1487, April 1994.

26. Obayashi, S.; and Guruswamy, G. P.: Convergence Acceleration of an Aeroelastic Navier–Stokes Solver. AIAA Paper 94-2268, June 1994.

27. Klopfer, G. H.; and Obayashi, S.: Virtual Zone Navier–Stokes Computations for Oscillating Control Surfaces. AIAA Paper 93-3363, July 1994.

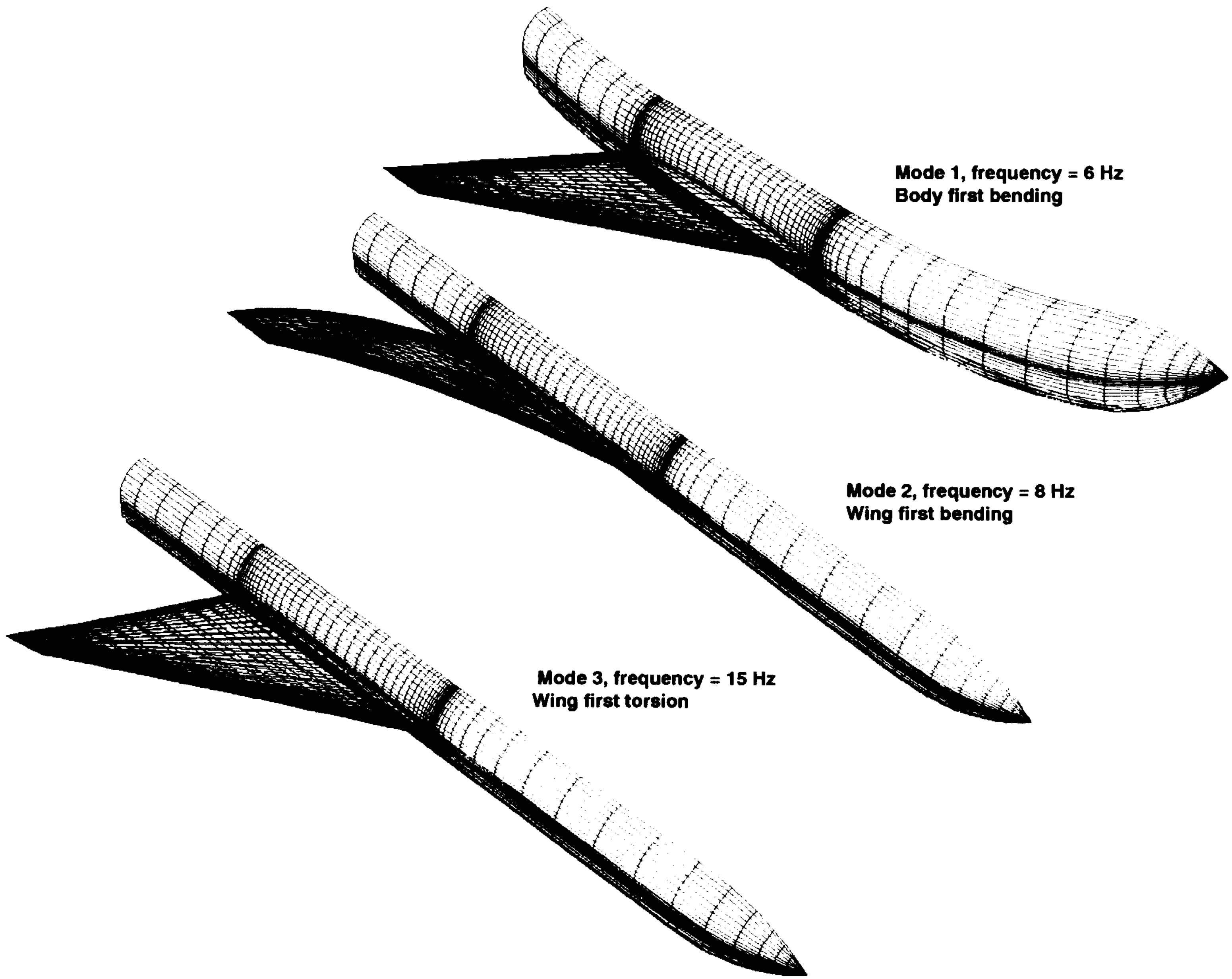

Figure 1. Mode shapes and frequencies of a wing-body configuration using the finite element method.

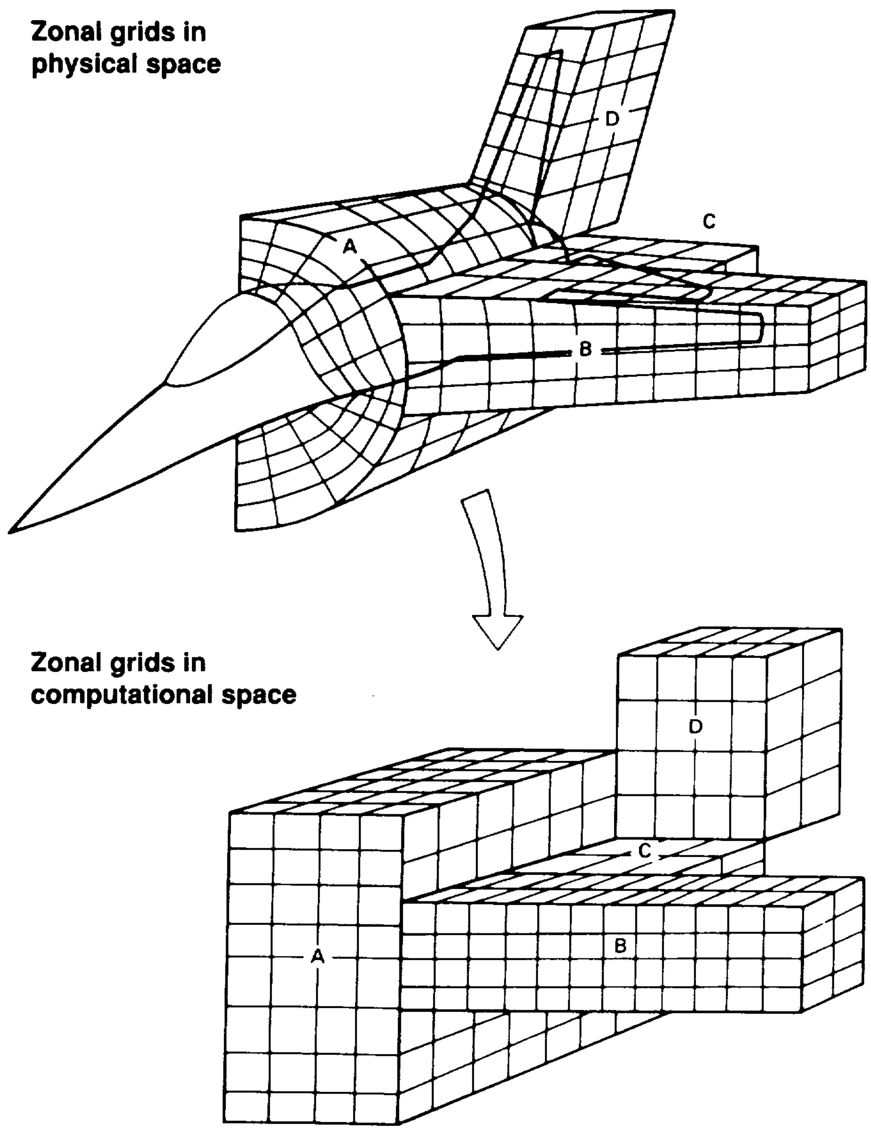

Figure 2. Body-conforming zonal grids of a fighter aircraft configuration in the physical and computational space.

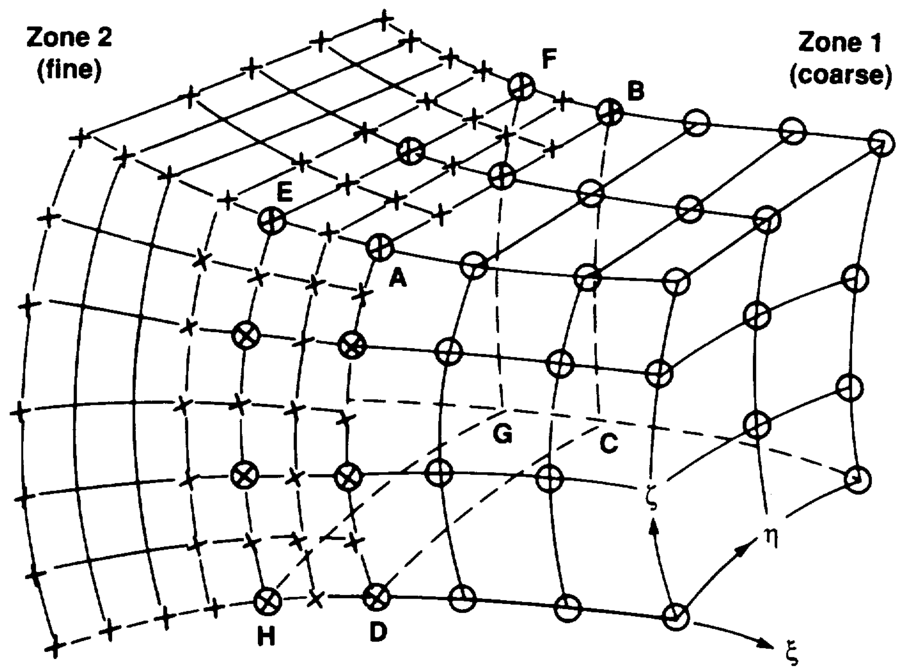

(a) Two-zone grid showing overlap at ABCD and EFGH planes in physical space

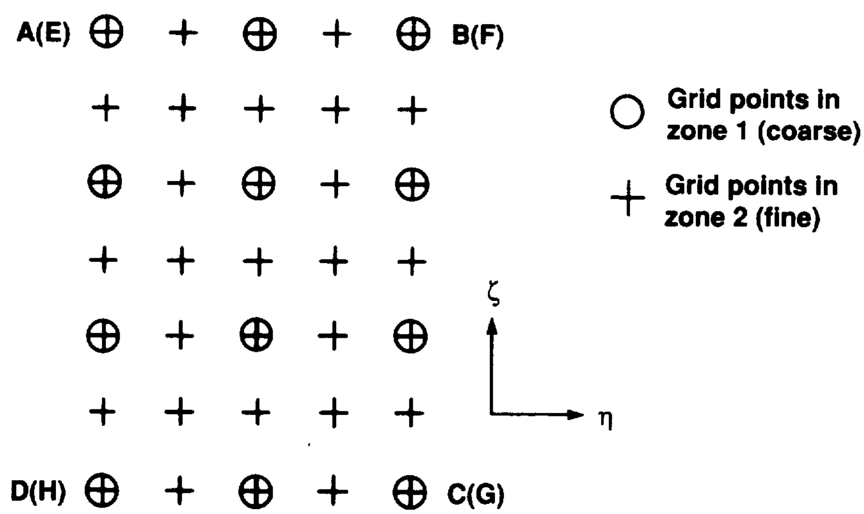

(b) Grid point detail in the overlap region in transformed space

Figure 3. Grid point details in the zonal interface region.

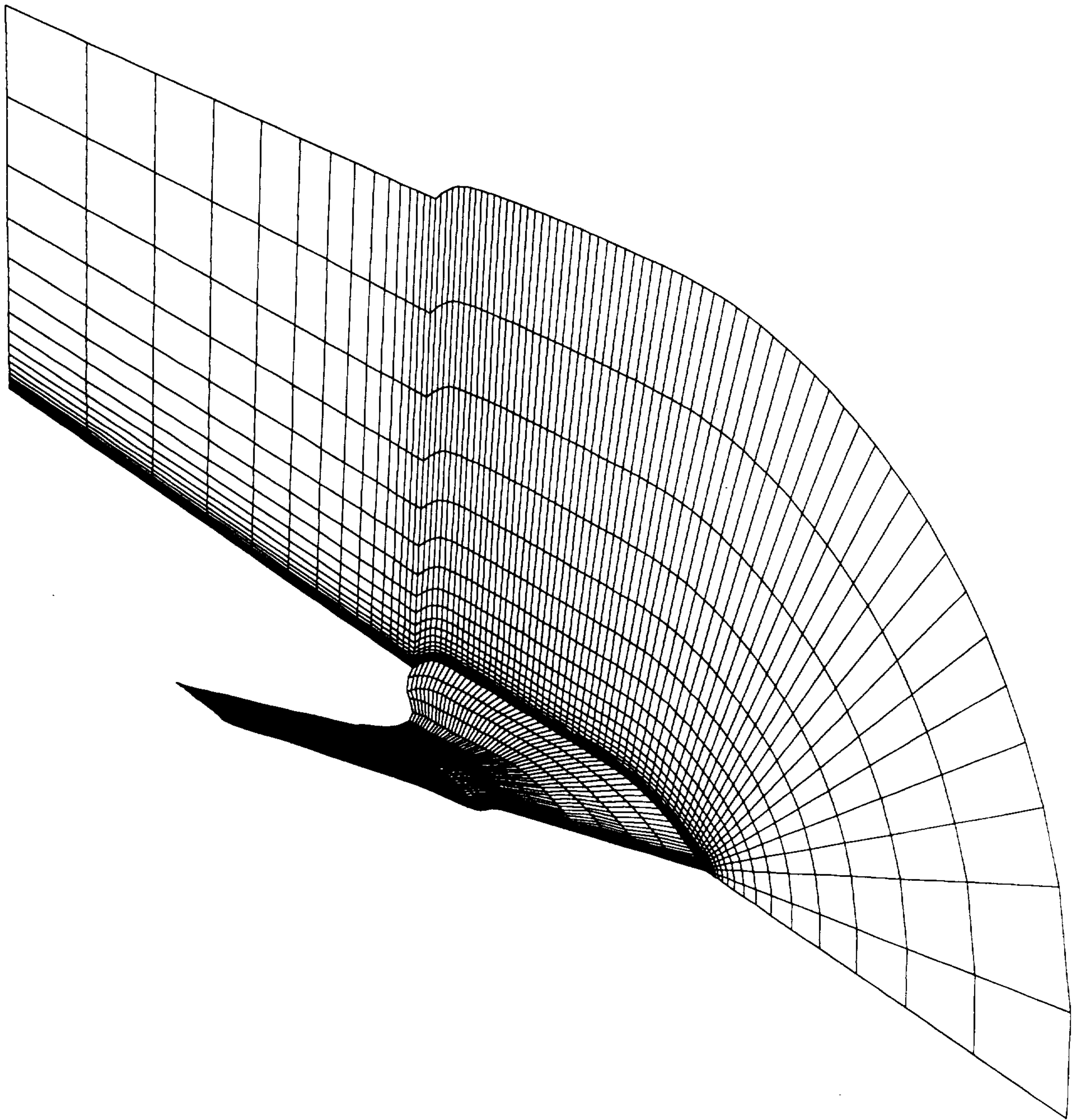

Figure 4. C-H-type grid for a typical blended wing-body configuration.

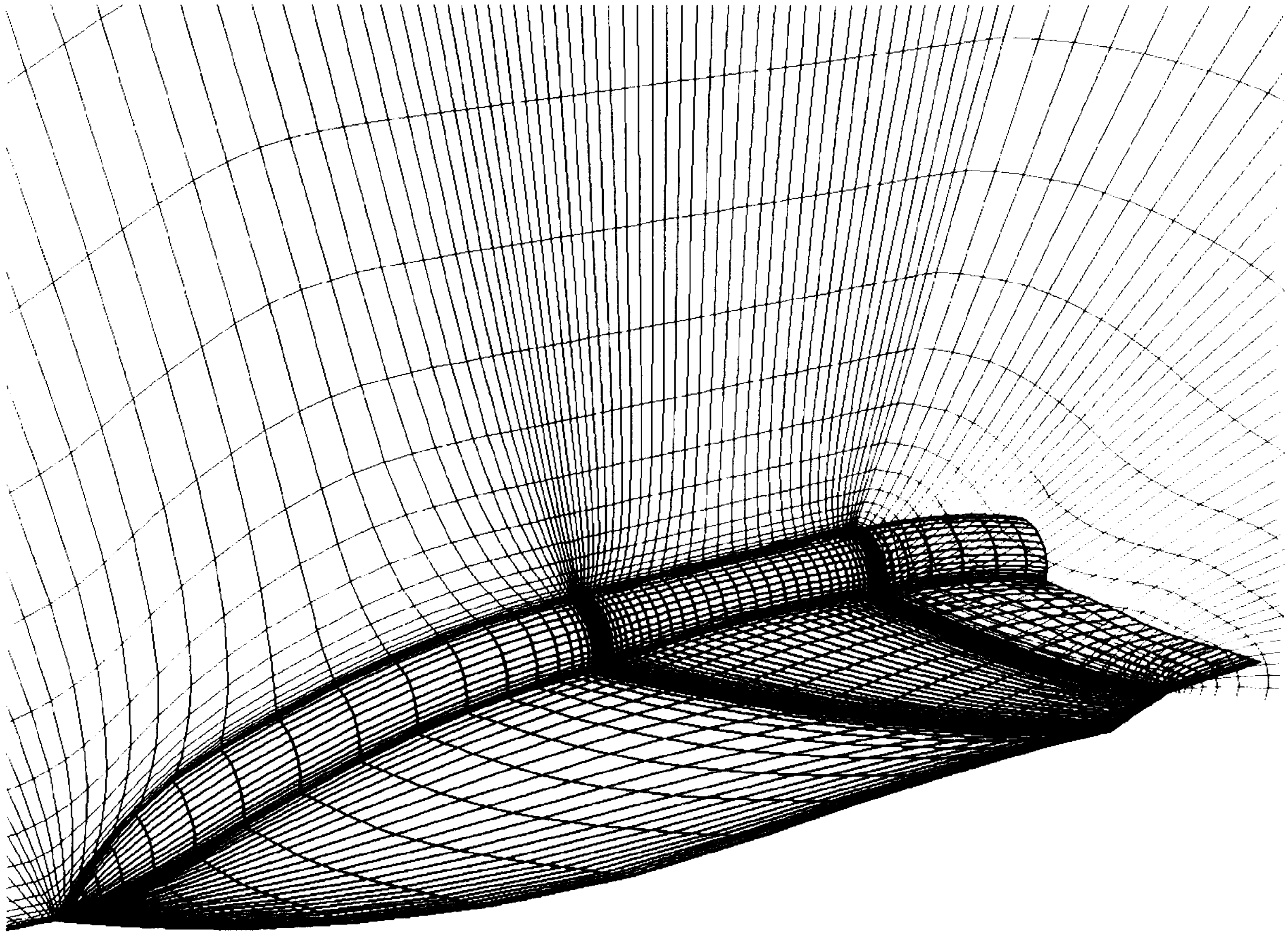

Figure 5. Aeroelastic configuration adaptive grid for a typical wing-body configuration.

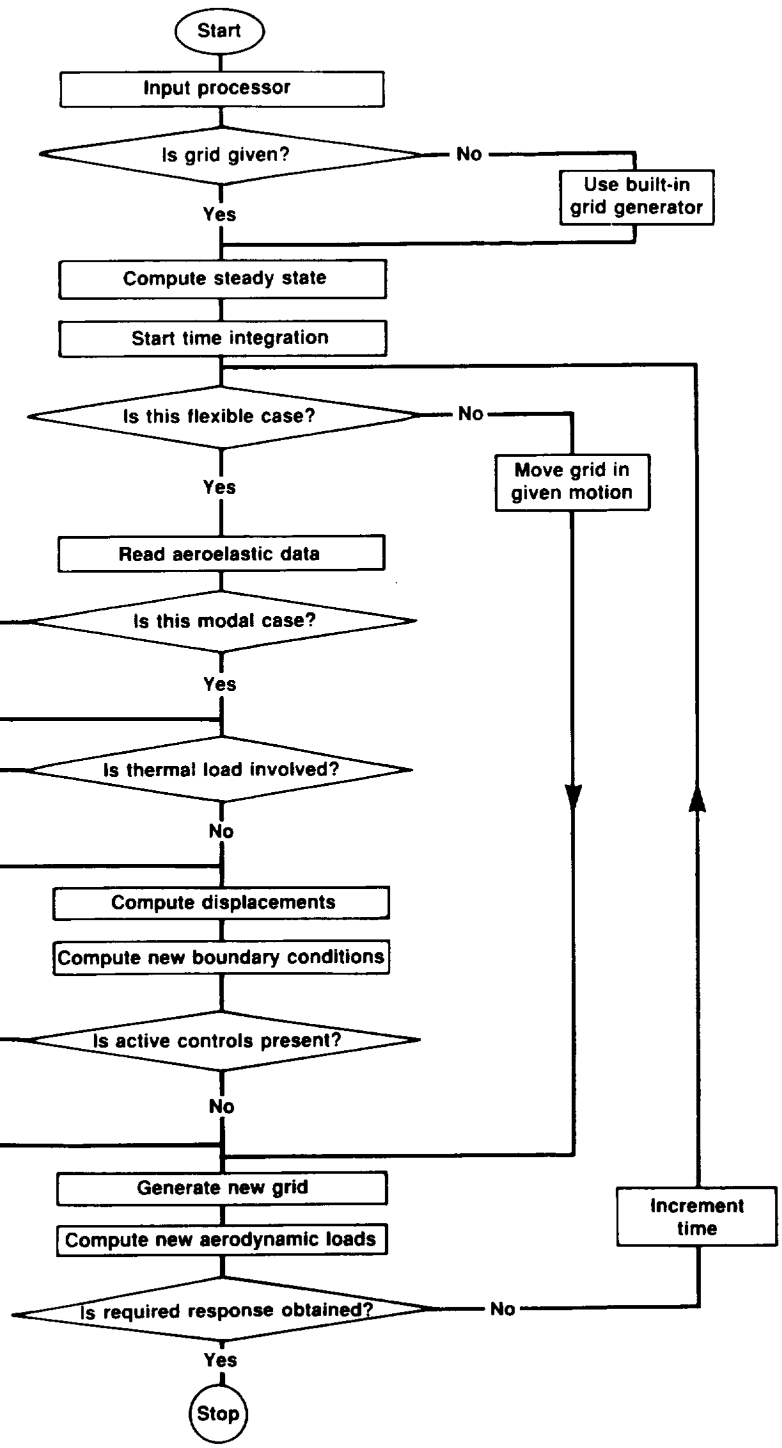

Figure 6. Flow diagram of ENSAERO.

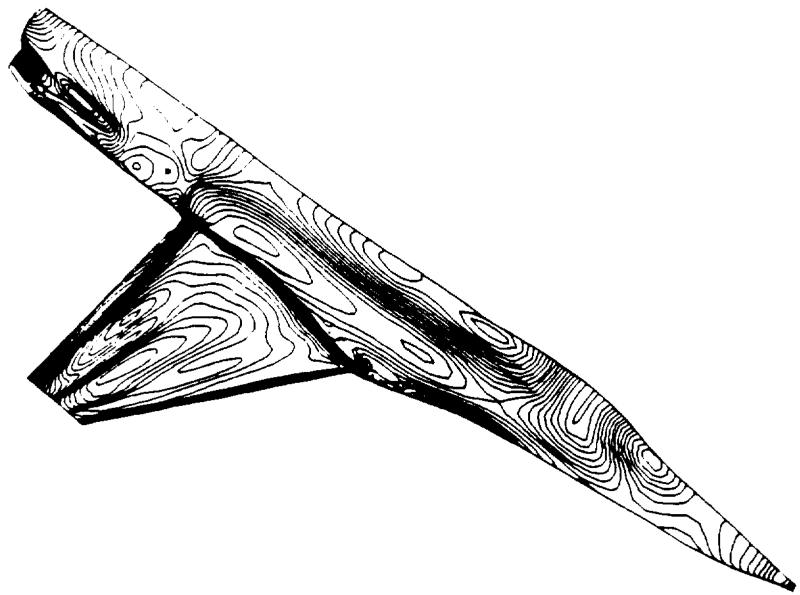

Figure 7. Mach contours of a typical wing-body configuration at M = 0.90, α = 1.69 deg, and Re = 4.5 $\times$ 10^6.

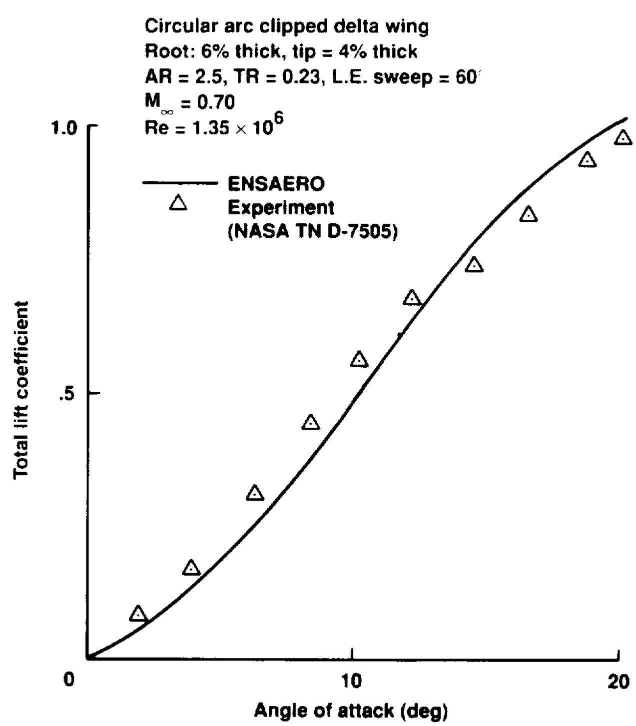

Figure 8. Comparison of computed lifts with the experiment.

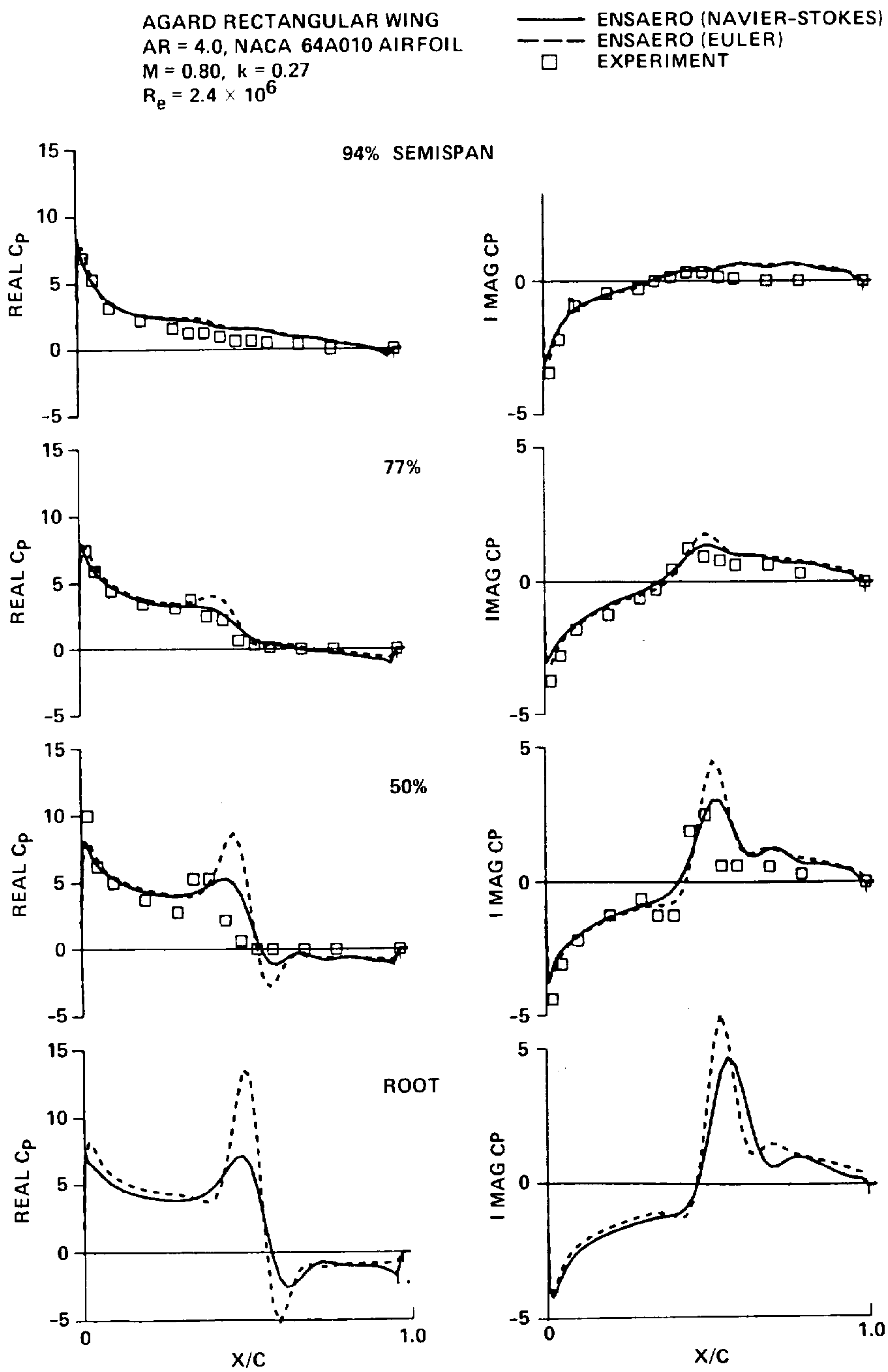

Figure 9. Comparison of Euler and Navier–Stokes unsteady pressures with the experiment.

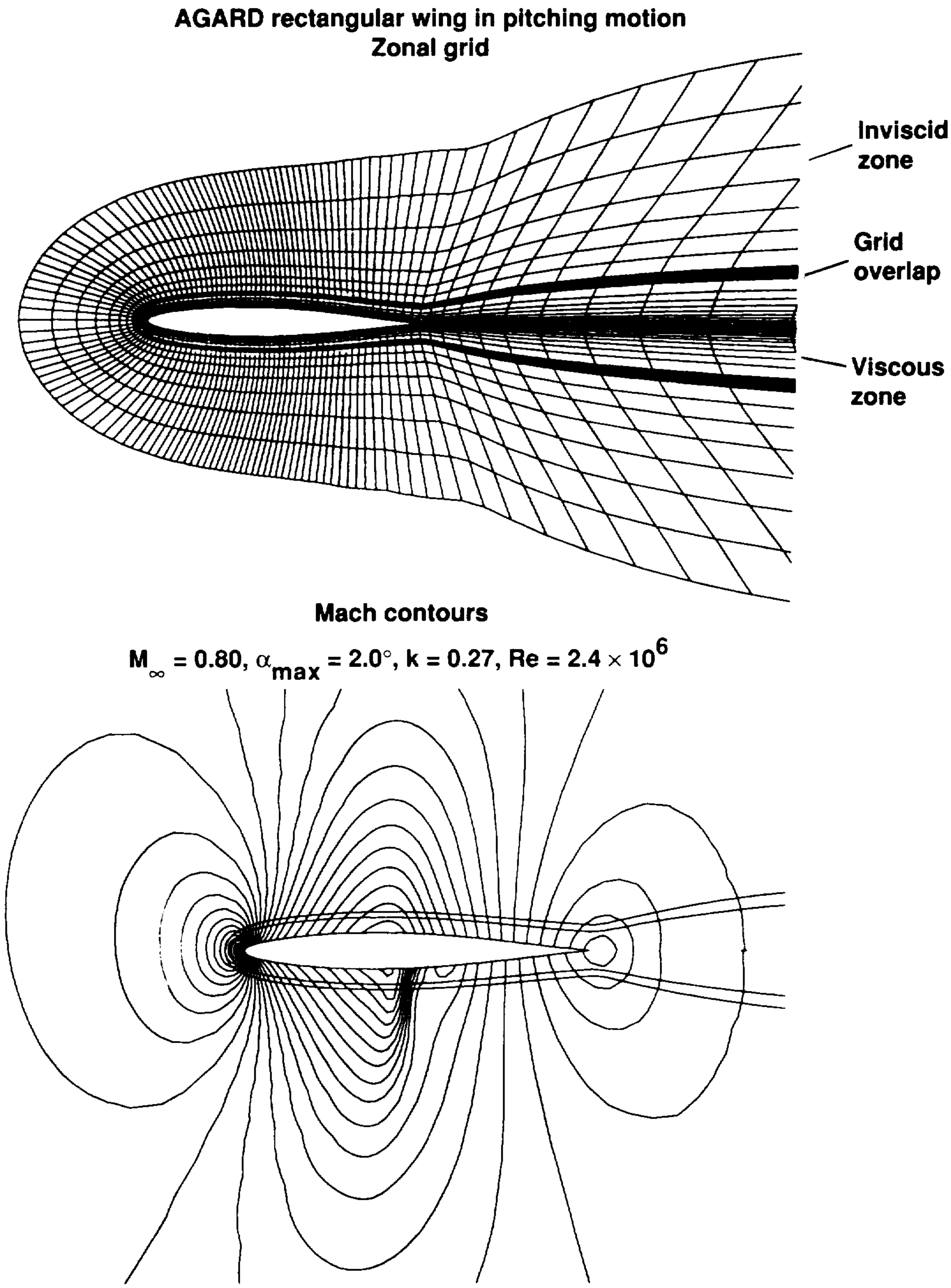

Figure 10. Mach contours at 50% semispan station using two-zone grid for an oscillating wing.

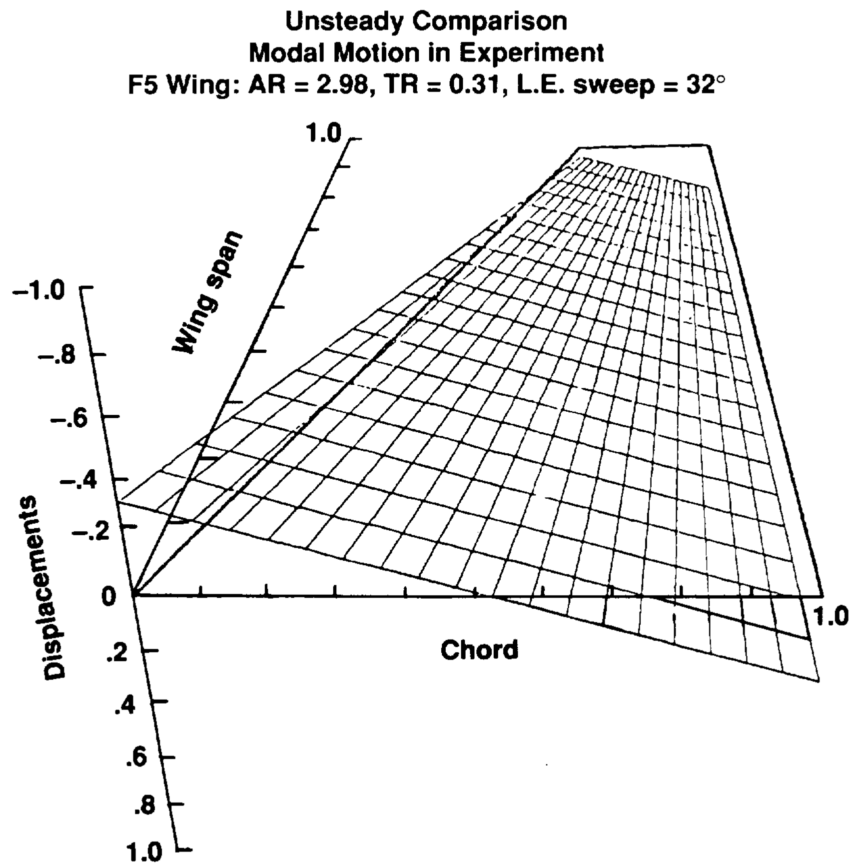

Figure 11. Unsteady motion of a rigid fighter wing.

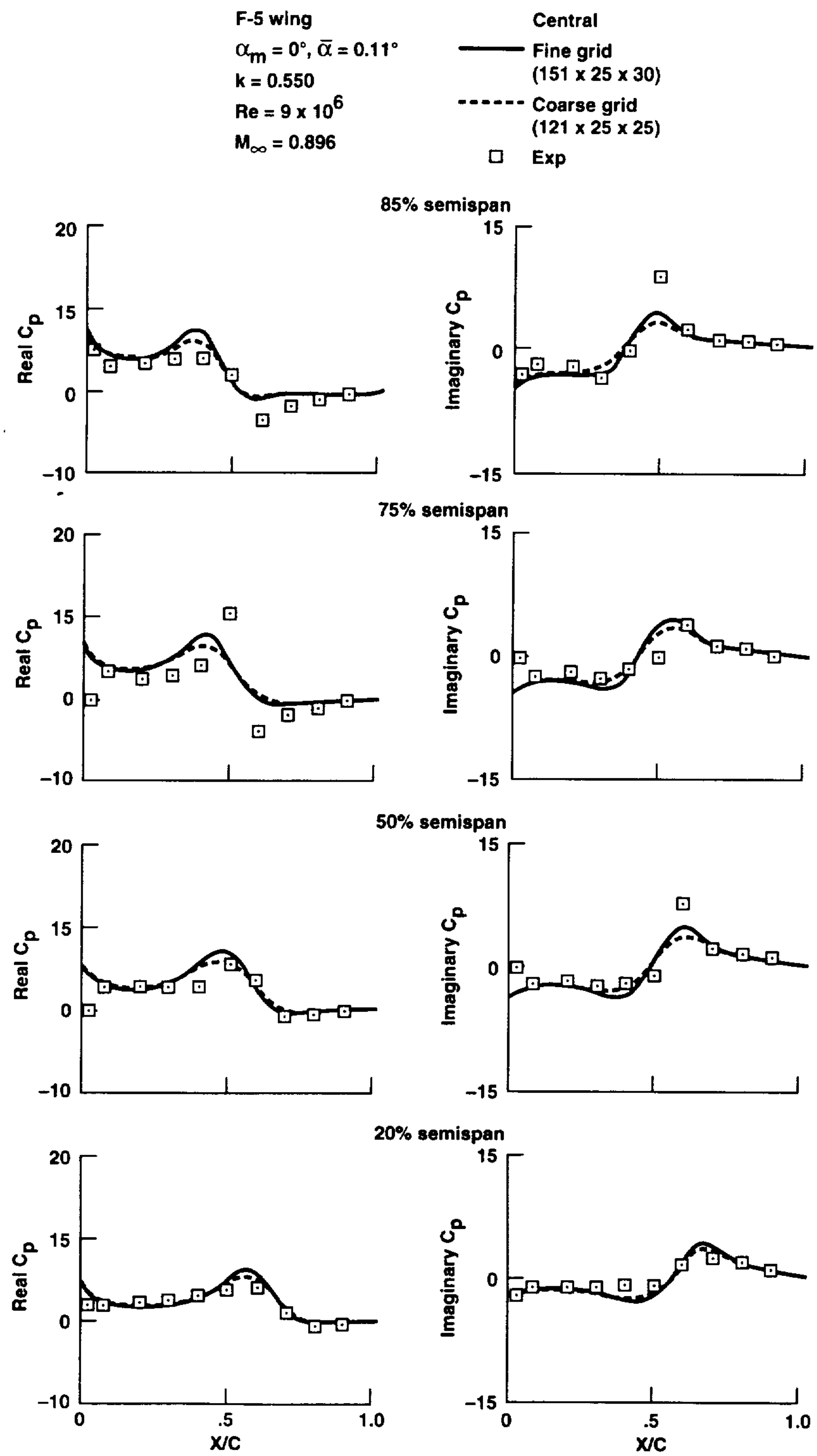

Figure 12. Comparison of the Navier–Stokes unsteady pressures with the experiment for a typical fighter wing.

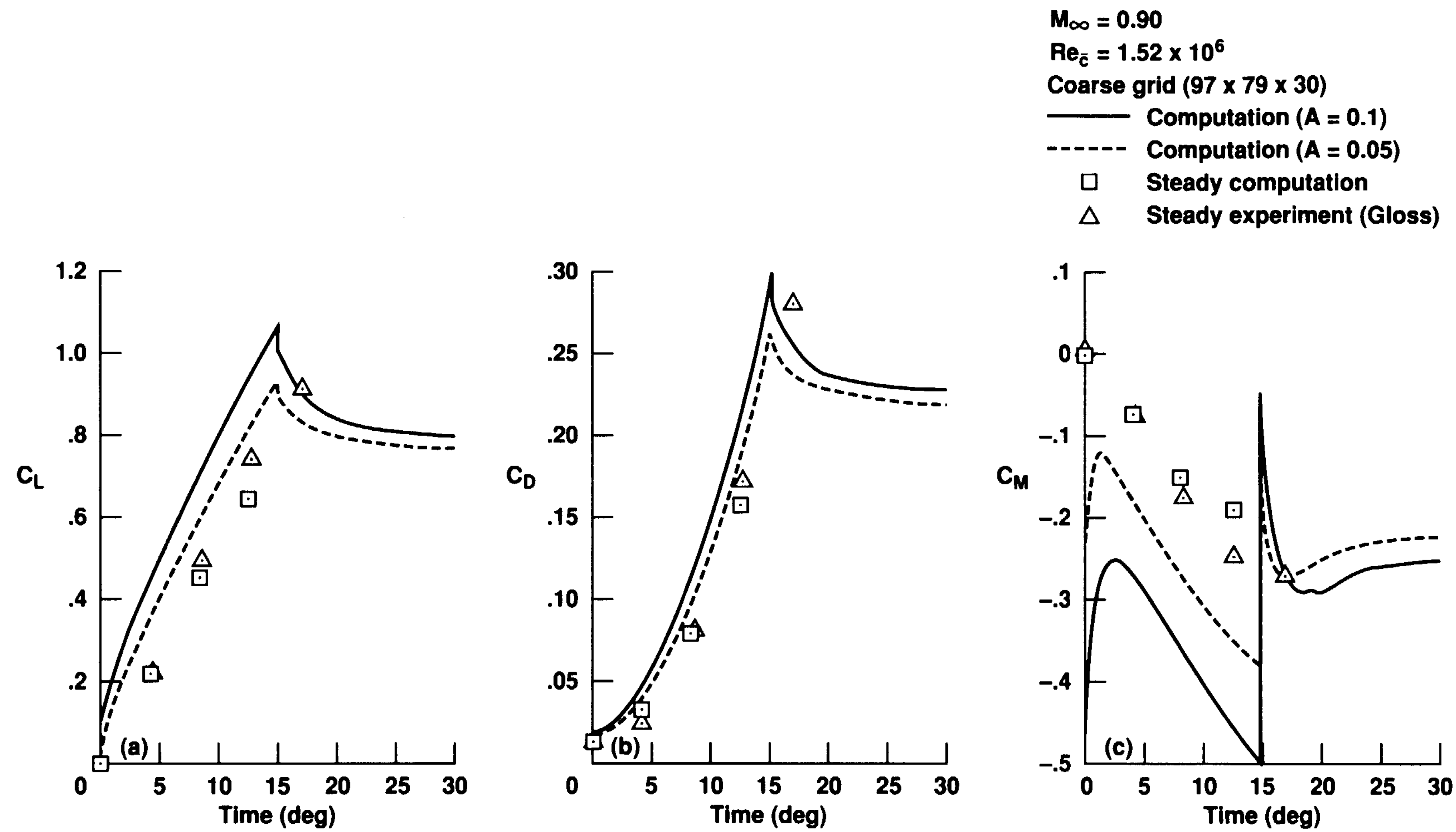

Figure 13. Unsteady surface pressure responses of a rigid wing-body configuration in ramp motion.

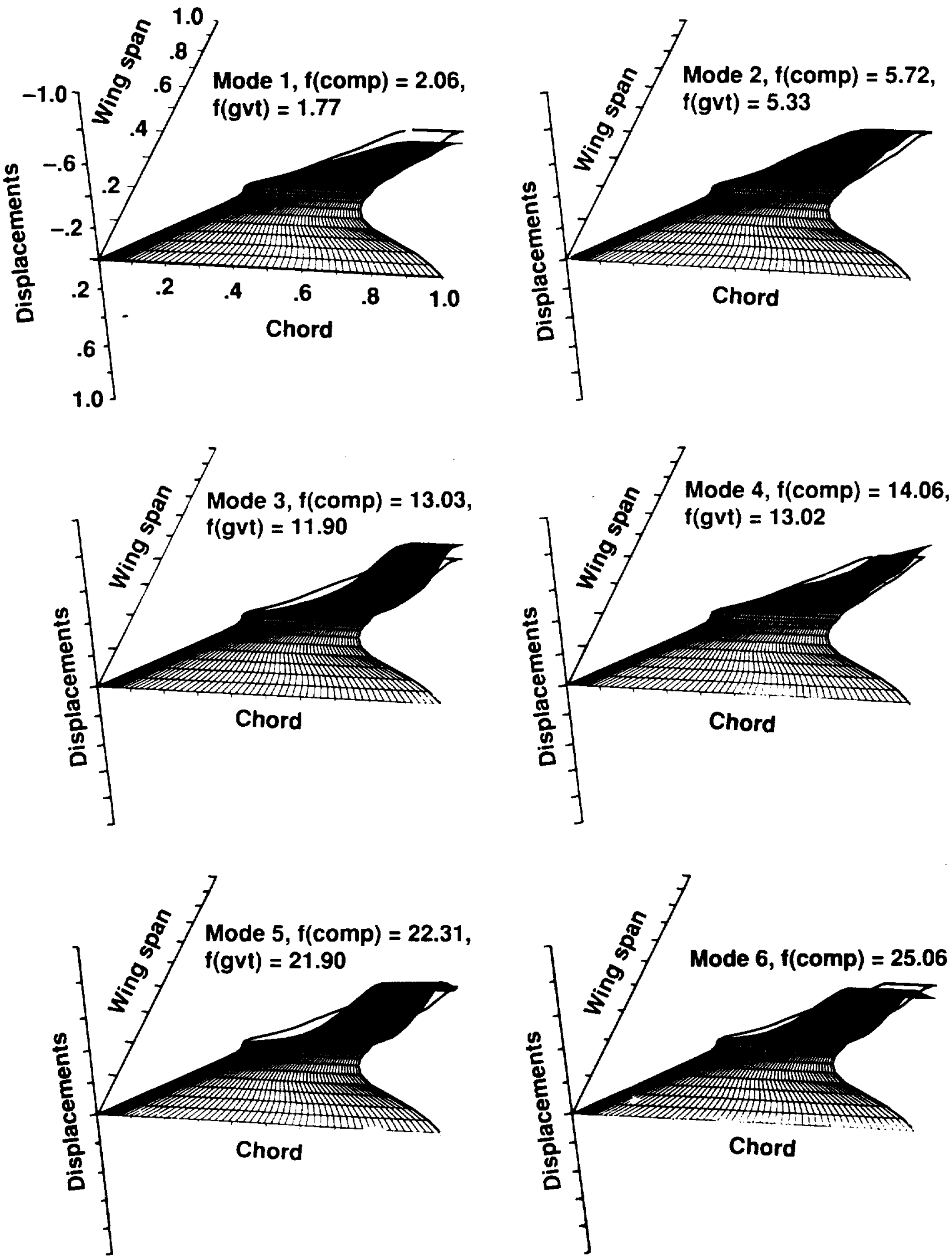

Figure 14. Mode shapes of a typical flexible blended wing-body configuration.

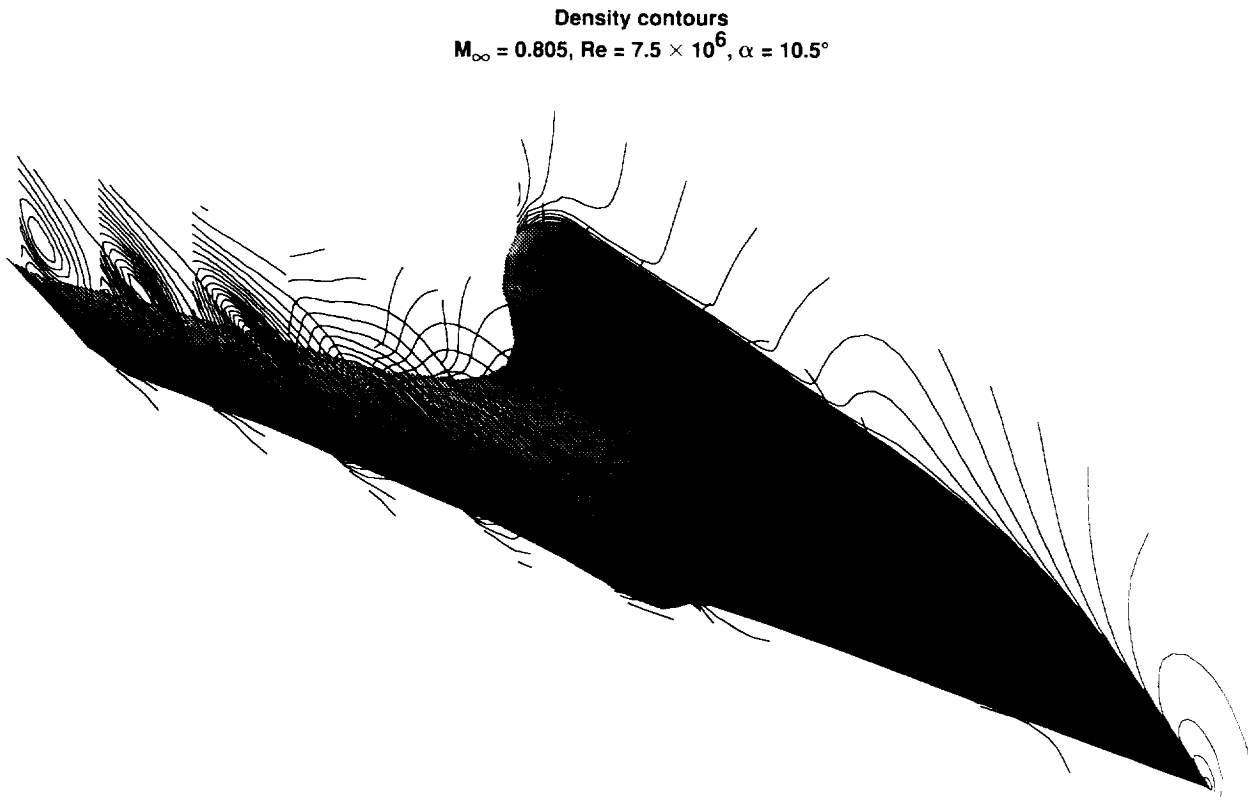

Figure 15. Velocity contours showing the presence of a strong vortex on the wing.

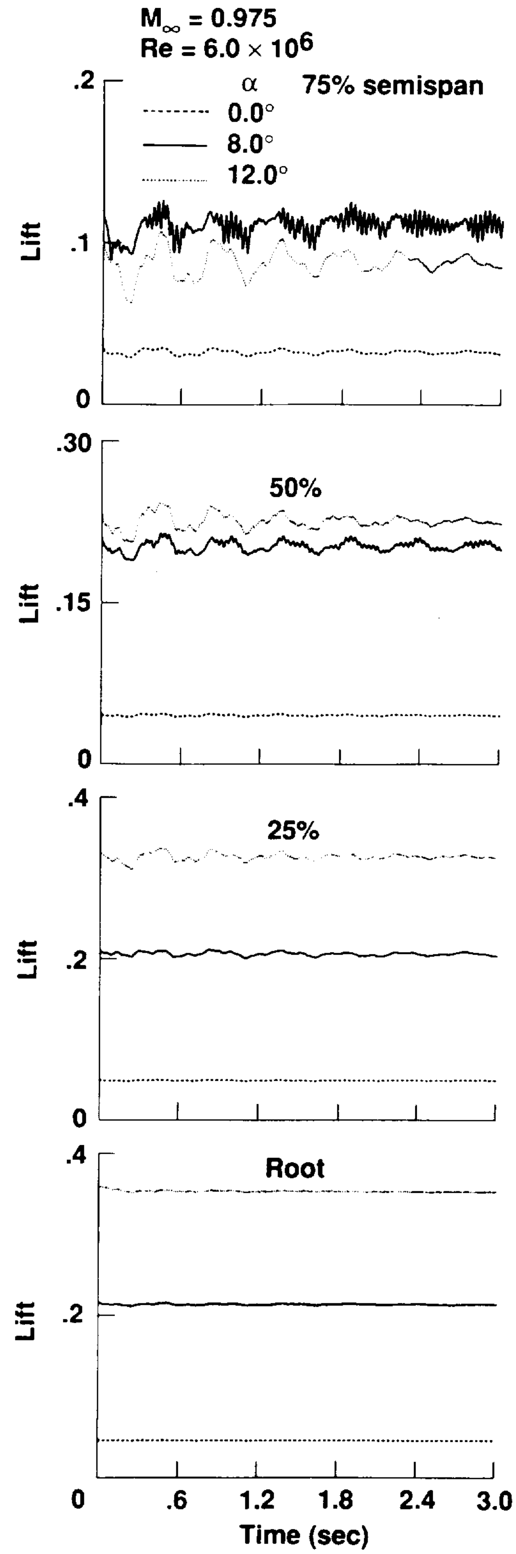

Figure 16. Effect of angle-of-attack on aeroelastic responses.

F-5 WING RESULTS

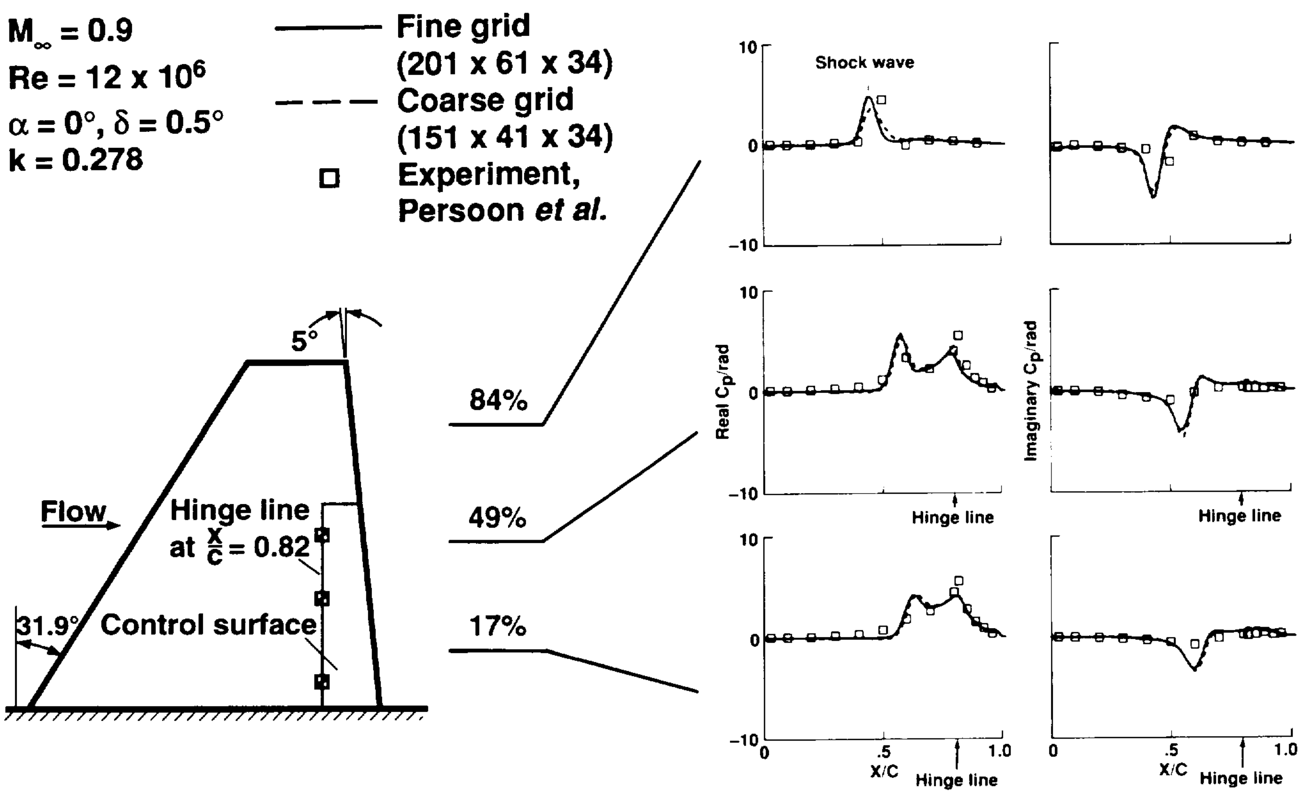

Figure 17. Comparison of unsteady pressures with experiment for a wing with oscillating control surface.

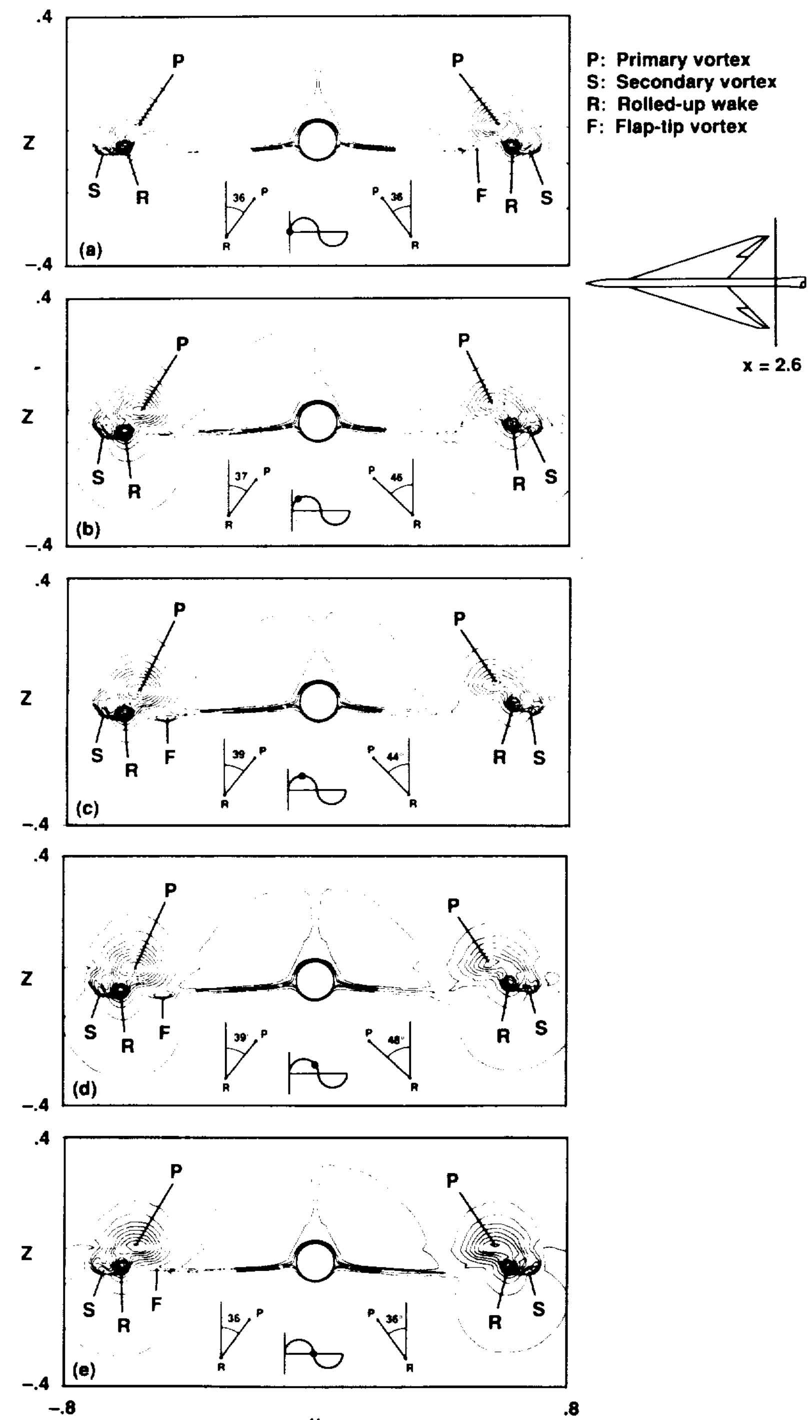

Figure 18. Effect of control surface oscillations on the leading edge vortices for a full-span wing-body configuration.

APPENDIX - A
USER'S MANUAL FOR ENSAERO

This version 2.3 includes options between central and upwind schemes
Built-in C-H Grid for Wings and Blended Wing-Bodies with moving Control Surfaces

GROUP NAME	VARIABLE	TYPE	DESCRIPTION
TITLE		HOLL	**Problem description**
	TITLE		In words
RESTA		INTG	**Flag for restarting**
*** comment line ***			
	IREAD		0 - Start from freestream conditions 1 - Start from steady/static-rigid 2 - Start from unsteady/dyn-aeroelastic conditions
	NBLK		Number of CFD zones
GRID			**Built-in C-H type grid**
*** comment line ***			
	JGRD	INTG	Number of points in x-direction
	KGRD	INTG	Number of points in y-direction
	LGRD	INTG	Number of points in z -direction
TASK	ITASK	INTG	**Flag for type of case**
*** comment line ***			
			0 - Steady rigid computations from steady 1 - Unsteady rigid computations from steady 2 - Unsteady rigid computations from unsteady 3 - Static aeroelastic computations 4 - Dynamic aeroelastic computations
FLOW		REAL	**Flow variables**
*** comment line ***			
	FSMACH		Mach number
	GAMMA		Ratio of specific heats
	RE		Reynolds number
	ALP		Angle of attack (freestream scaling in deg)
	TINF		Freestream temperature for Sutherland Law (negative value disables this option)
DISP		REAL	**Dissipation values**
*** comment line ***			
	DIS2		Second order dissipation
	DIS4		Fourth order dissipation

default is the diagonal form Beam-Warming central differencing
set DIS2 and DIS4 to less than zero to invoke streamwise upwind option

VISC		INTG	**Flags for viscous options**
*** comment line ***			
	IVIS		Global flag
			0 Inviscid Euler calculations
			1 Viscous Navier-Stokes calculations
	IVISK		Flag for spanwise viscous terms
			0 OFF
			1 ON
	IVISL		Flag for normal viscous terms
*** comment line ***			
			0 - OFF
			1- ON
TURB		INTG	**Flags for turbulence modeling**
*** comment line ***			
	ITURB		0 - Laminar calculations
			1 - Baldwin-Lomax turbulence model
ISPE		INTG	**Variables for special options**
*** comment line ***			
	IDSM		0 - Original Baldwin-Lomax model
			1 - Correction for vortical flows
ITER		INTG	**Variables to set number of time steps**
*** comment line ***			
	NSTART		Starting time step
	NSTOP		Ending time step
PFLAG		INTG	**Flags to control outputs**
*** comment line ***			
	IPRGRD		Freq. of grid output to unit 2
	IPRPRE		Freq. of pressure output to unit 6
	IPRPLT		Freq. of grid and q output to unit 2 and 3
	IPRAER		Freq. of aeroelastic output to unit 13
*** comment line ***			
XGRID		MIXED	**Input for to x-grid generation**
	NXIN	INTG	No. of x points from l.e. to downstream
	NXIW	INTG	No. of x pts on wing surface (mult of 4)
	NLTRA	INTG	X index of the t.e. (lower)
	NUTRA	INTG	X index of the t.e. (upper)
	XMAX	REAL	Maximum value of x-grid in downstream
	XEXP	REAL	Expo. stretching factor for x-grid after t.e.

	SNOS	REAL	Spacing at the l.e.
	STRA	REAL	Spacing at the t.e.
ZGRID		REAL	**Input for z-grid**
*** comment line ***			
	ZFIS	REAL	Spacing near the surface
	ZEXP	REAL	Expo. stretching factor for z-grid
WDATA			**Input to define wing planform**
*** comment line ***			
	IRATIO	INTG	Flag to define the type of planform data 1 Input in ratios 2 Input in co-ordinates
	ICONTR	INTG	Flag to define the type of planform data 0 Control surface off 1 Control surface on
if IRATIO = 1 then read input in ratios as			
*** comment line ***			
	INDTIP	INTG	Y-index of the wing tip
	ARATIO	REAL	Aspect ratio based on full span
	TRATIO	REAL	Taper ratio
	SWANGL	REAL	L.E. Sweep angle in deg
if IRATIO = 2 then read input in co-ordinates as			
*** comment line ***			
	INDTIP	INTG	Y-index of the wing tip
*** comment line ***			
	YDIS	REAL	Span station values of KGRD span sections
	XLE	REAL	Leading edge X values of KGRD span sections
	CHORD	REAL	Chord values of KGRD span sections
this data is needed only if ICONTR = 1			
CONDAT		MIXED	**Input to define control surface**
*** comment line ***			
	IGRAL		0 - Sheared grid for moving control surface 1 - Algebraic grid for moving control surface
	XTRCN	REAL	X/C value of control surface hinge
	YTRCN1	REAL	Inboard location of control surface hinge
	YTRCN2	REAL	Outboard location of control surface hinge
	KTRCN1	INTG	Inboard span index of control surface hinge
	KTRCN2	INTG	Outboard span index of control surface hinge
SCADAT			**Input to define wing thickness**
*** comment line ***			
	YSCA	REAL	Scale for wing thickness at KGRD stations
AIRDAT			**Input to define wing section**
*** comment line ***			
	IAIR	INTG	Flag to define type of airfoil

			= 1 Circular arc of thickness ratio THK = 2 Polynomial input data = 3 Co-ordinate input data for variable sections
if IAIR = 1 read			
*** comment line ***			
	THK	REAL	Thickness ratio of circular arc airfoils
if IAIR = 2 read coefficients of polynomials			
*** comment line ***			
	A0, A1, A2, A3, A4, A5	REAL	Coefs. of the thickness funcs
*** comment line ***			
	B1, B2, B3, B4, B5	REAL	Coefs. of the camber funcs
if IAIR = 3 read			
*** comment line ***			
	NAIRSEC	INTG	Number of airfoil sections
for NAIRSEC sections repeat			
*** comment line ***			
	IDUM	INTG	Section number
	NINU	INTG	Number of points to define upper surface
	NINL	INTG	Number of points to define lower surface
	YINP	REAL	Span station value of the given section
*** comment line ***			
	XINU	REAL	NINU x values upper surface points
*** comment line ***			
	ZINU	REAL	NINU z values upper surface points
*** comment line ***			
	XINL	REAL	NINL x values lower surface points
*** comment line ***			
	XINL	REAL	NINL z values lower surface points

TWSDAT			**Rigid and twist angles**
*** comment line ***			
	SANG	REAL	Rigid angle of attack
*** comment line ***			
	TWSANG	REAL	KDIMC values of twist angles

UNSDAT			**Input for unsteady rigid motion**
*** comment line ***			
	REDFRE	REAL	Reduced frequency based on chord
	PHAA	REAL	Phase lag in deg for pitch motion
	PAXIS	REAL	Axes for pitch motion
	PHAD	REAL	Phase lag in deg for plunge motion
	FORAMP	REAL	Scale factor for fourier coefficients
	PRAT	REAL	Pitch rate for ramp motion
	RAMANG	REAL	Maximum ramp angle of attack
	MTYPE	INTG	Flag to control motion type

			= 0 Steady case
			= 1 Unsteady sinusoidal case
			= 2 Unsteady ramp case
	MODINP	INTG	Flag to control modal data type
			= 1 Modal data in shape format
			= 2 Modal data in sectional value format
	NSPC	INTG	Number of time steps per cycle
if MODINP equal to 1 read following modal data			
*** comment line ***			
	JMOD	INTG	No. of data points in x direction
	KMOD	INTG	No. of data points in y direction
*** comment line ***			
	RMODX	REAL	Array of x-locations for modal data
*** comment line ***			
	RMODY	REAL	Array of y-locations for modal data
*** comment line ***			
	RIGMOD	REAL	Read matrix of modal displacements
if MODINP equal to 2 read following modal data			
*** comment line ***			
	BENSCA	REAL	Value of tip displacement in root chord for the first bending mode
*** comment line ***			
	PITDIS	REAL	Array of length KGRD containing amplitudes of sectional angles-of-attack in deg
if ITASK equal to 3 or 4 read following aeroelastic data			
this data is needed only if ICONTR = 1			
UNSCON			**Input for control surface motion**
*** comment line ***			
	RKTRCN	REAL	Reduced freq based on chord for control surface
	PDTRCN	REAL	Control surface amplitude in radians
AERDAT			**Aeroelastic input data**
	PHYLEN	REAL	Characteristic length in inches
	DYNPRE	REAL	Dynamic pressure (psi)
	FREVEL	REAL	Freestream velocity in/sec
*** comment line ***			
	NMODES	INTG	Number of modes
	NXMOD	INTG	No. of data points in x direction
	NYMOD	INTG	No. of data points in y direction
*** comment line ***			
	XMOD	REAL	Array of x-locations for modal data
*** comment line ***			
	YMOD	REAL	Array of y-locations for modal data
repeat following data till all modes are completed			
*** comment line ***			
repeat following data till all spans are completed			
*** comment line ***			
	DISP	REAL	Array of modal displacements along x-locations

endrepeat

*** comment line ***		
GENMAS	REAL	(NMODESxNMODES) gen. mass matrix
*** comment line ***		
GENDAM	REAL	(NMODESxNMODES) gen. damping matrix
*** comment line ***		
GENSTF	REAL	(NMODESxNMODES) gen. stiffness matrix
*** comment line ***		
GENDII	REAL	(NMODES) initial gen. displacement vector
*** comment line ***		
GENVEI	REAL	(NMODES) initial gen. velocity vector
*** comment line ***		
GENACI	REAL	(NMODES) initial gen. accn. vector

INPUT AND OUTPUT FILES

UNIT	DATA TYPE	CONTENTS
2	FORMATTED	Grid on wing only for dynamic cases
3	FORMATTED	Q on wing only for dynamic cases
6	FORMATTED	Detailed echo of input and several output data
11	FORMATTED	Residual output
12	FORMATTED	Debug summary (negative jacobians)
21	UNFORMATTED	Input Restart file (Q and grid in PLOT3D format)
22	UNFORMATTED	Output Restart file (Q and grid in PLOT3D format)
34	FORMATTED	Force coefficients every 10 time steps

NOTE

Enter input using free format with one line per group.
Comment lines are required to be read-in between groups.
Italics provides additional notes for each data group.

APPENDIX - B

```
SAMPLE CASE OF A WING WITH OSCILLATING CONTROL SURFACE
RESTART  0(START) 1 (START FROM DIFFERENT TASK) 2 (   FROM SAME TASK), ZONES
0,                                                                      1
GRID JGRD  KGRD  LGRD
     151,   44,    34
TASK  0 = STD, 1= UNS FROM STD, 2 = UNS, 3= STATIC AERO, 4= DYNAMIC AERO.
      0
FLOW VARIABLES   FSMACH,  GAMMA,  RE,     ALP  TEMP
                   0.854,    1.135,  0.0,    0.,   0.0
DISSIPATIONS     DIS2,    DIS4
                  0.25,    0.02
VISCOUS OPTIONS GLOBAL, K-DIRECTION, L-DIRECTION
                   0,        0,          0
TURBULANCE OPTION 0 = OFF, 1 = ON
                   0
ALGORITHM FLAGS: FREESTREAM CAPTURING, REGENERATION FOR CONTROL,
DEGANI-SCHIFF
                   0,                       1,                          0
TIME STEPS      START  STOP
                  1,  10
PRINT FLAGS IPRGRD(grid)   IPRPRE (pre), IPLTFRE(plot), IAERPRE(AERO)
                  1,        1000,        100000,        10000
X GRID DATA  NXIN,NXIW,NLTRA,NUTRA,    XMAX, XEXP,  SNOS,  STRA
               75,   60,    16,   136,      3.0,   1.2,  0.008,  0.02
Z GRID DATA  ZMAX, EXPONENT
            0.005,   1.15
PLANFORM FORMAT 1 = RATIOS, 2 = CO-ORDINATES CONTROL SURFACE 0 = OFF, 1 = ON
                 1,                                                       1
 WING DATA   TIP INDEX (INDTIP)  AR     TR              LE SWEEP ANGLE
                    34,             3.0,   0.142857143, 51.34019175
 CONTROL SURFACE : IGRAL,X/C, SPAN INBOARD,OUTBOARD (2y/b), INDECES K1,K2
                    0,  .80,  0.566,            0.829,                13, 25
 YSCA
    0.1000E+01,  0.1000E+01,   0.1000E+01,   0.1000E+01,   0.1000E+01,
    0.1000E+01,  0.1000E+01,   0.1000E+01,   0.1000E+01,   0.1000E+01,
    0.1000E+01,  0.1000E+01,   0.1000E+01,   0.1000E+01,   0.1000E+01,
    0.1000E+01,  0.1000E+01,   0.1000E+01,   0.1000E+01,   0.1000E+01,
    0.1000E+01,  0.1000E+01,   0.1000E+01,   0.1000E+01,   0.1000E+01,
    0.1000E+01,  0.1000E+01,   0.1000E+01,   0.1000E+01,   0.1000E+01,
    0.1000E+01,  0.8888E+00,   0.4444E+00,   0.0001E-02,   0.0001E-02,
```

0.0001E-02, 0.0001E-02, 0.0001E-02, 0.0001E-02, 0.0001E-02,
0.0001E-02, 0.0001E-02, 0.0001E-02, 0.0001E-02

AIRFOIL DATA IAIR (1 PARABOLIC ARC, 2 = GENERAL FUNCTIONS, 3 = COORDINATES)
3

NO OF SECTIONS
2

SEC No., NINU, NINL, YVAL
1 34, 34, 0.0

XINU

0.000000E+00	0.500000E-03	0.100000E-02	0.150000E-02	0.200000E-02
0.250000E-02	0.300000E-02	0.350000E-02	0.400000E-02	0.500000E-02
0.750000E-02	0.125000E-01	0.250000E-01	0.500000E-01	0.750000E-01
0.100000E+00	0.150000E+00	0.200000E+00	0.250000E+00	0.300000E+00
0.350000E+00	0.400000E+00	0.450000E+00	0.500000E+00	0.550000E+00
0.600000E+00	0.650000E+00	0.700000E+00	0.750000E+00	0.800000E+00
0.850000E+00	0.900000E+00	0.950000E+00	0.100000E+01	

ZINU

0.000000E+00	0.151536E-02	0.213197E-02	0.260057E-02	0.299247E-02
0.333529E-02	0.364320E-02	0.392462E-02	0.418504E-02	0.464000E-02
0.563000E-02	0.718000E-02	0.981000E-02	0.131300E-01	0.159100E-01
0.182400E-01	0.219400E-01	0.247400E-01	0.268700E-01	0.284200E-01
0.294500E-01	0.299600E-01	0.299200E-01	0.292500E-01	0.279300E-01
0.260200E-01	0.236400E-01	0.208700E-01	0.177500E-01	0.143700E-01
0.108300E-01	0.727000E-02	0.370000E-02	0.130000E-03	

XINL

0.000000E+00	0.500000E-03	0.100000E-02	0.150000E-02	0.200000E-02
0.250000E-02	0.300000E-02	0.350000E-02	0.400000E-02	0.500000E-02
0.750000E-02	0.125000E-01	0.250000E-01	0.500000E-01	0.750000E-01
0.100000E+00	0.150000E+00	0.200000E+00	0.250000E+00	0.300000E+00
0.350000E+00	0.400000E+00	0.450000E+00	0.500000E+00	0.550000E+00
0.600000E+00	0.650000E+00	0.700000E+00	0.750000E+00	0.800000E+00
0.850000E+00	0.900000E+00	0.950000E+00	0.100000E+01	

ZINL

0.000000E+00	-0.151536E-02	-0.213197E-02	-0.260057E-02	-0.299247E-02
-0.333529E-02	-0.364320E-02	-0.392462E-02	-0.418504E-02	-0.464000E-02
-0.563000E-02	-0.718000E-02	-0.981000E-02	-0.131300E-01	-0.159100E-01
-0.182400E-01	-0.219400E-01	-0.247400E-01	-0.268700E-01	-0.284200E-01
-0.294500E-01	-0.299600E-01	-0.299200E-01	-0.292500E-01	-0.279300E-01
-0.260200E-01	-0.236400E-01	-0.208700E-01	-0.177500E-01	-0.143700E-01
-0.108300E-01	-0.727000E-02	-0.370000E-02	-0.130000E-03	

SEC No., NINU, NINL, YVAL
2 34, 34, 1.0

XINU

```
   0.000000E+00   0.500000E-03   0.100000E-02   0.150000E-02   0.200000E-02
   0.250000E-02   0.300000E-02   0.350000E-02   0.400000E-02   0.500000E-02
   0.750000E-02   0.125000E-01   0.250000E-01   0.500000E-01   0.750000E-01
   0.100000E+00   0.150000E+00   0.200000E+00   0.250000E+00   0.300000E+00
   0.350000E+00   0.400000E+00   0.450000E+00   0.500000E+00   0.550000E+00
   0.600000E+00   0.650000E+00   0.700000E+00   0.750000E+00   0.800000E+00
   0.850000E+00   0.900000E+00   0.950000E+00   0.100000E+01
ZINU
   0.000000E+00   0.151536E-02   0.213197E-02   0.260057E-02   0.299247E-02
   0.333529E-02   0.364320E-02   0.392462E-02   0.418504E-02   0.464000E-02
   0.563000E-02   0.718000E-02   0.981000E-02   0.131300E-01   0.159100E-01
   0.182400E-01   0.219400E-01   0.247400E-01   0.268700E-01   0.284200E-01
   0.294500E-01   0.299600E-01   0.299200E-01   0.292500E-01   0.279300E-01
   0.260200E-01   0.236400E-01   0.208700E-01   0.177500E-01   0.143700E-01
   0.108300E-01   0.727000E-02   0.370000E-02   0.130000E-03
XINL
   0.000000E+00   0.500000E-03   0.100000E-02   0.150000E-02   0.200000E-02
   0.250000E-02   0.300000E-02   0.350000E-02   0.400000E-02   0.500000E-02
   0.750000E-02   0.125000E-01   0.250000E-01   0.500000E-01   0.750000E-01
   0.100000E+00   0.150000E+00   0.200000E+00   0.250000E+00   0.300000E+00
   0.350000E+00   0.400000E+00   0.450000E+00   0.500000E+00   0.550000E+00
   0.600000E+00   0.650000E+00   0.700000E+00   0.750000E+00   0.800000E+00
   0.850000E+00   0.900000E+00   0.950000E+00   0.100000E+01
ZINL
    0.000000E+00  -0.151536E-02  -0.213197E-02  -0.260057E-02  -0.299247E-02
   -0.333529E-02  -0.364320E-02  -0.392462E-02  -0.418504E-02  -0.464000E-02
   -0.563000E-02  -0.718000E-02  -0.981000E-02  -0.131300E-01  -0.159100E-01
   -0.182400E-01  -0.219400E-01  -0.247400E-01  -0.268700E-01  -0.284200E-01
   -0.294500E-01  -0.299600E-01  -0.299200E-01  -0.292500E-01  -0.279300E-01
   -0.260200E-01  -0.236400E-01  -0.208700E-01  -0.177500E-01  -0.143700E-01
   -0.108300E-01  -0.727000E-02  -0.370000E-02  -0.130000E-03
RIGID ANGLE
0.0
TWIST ANGLES
0.0, 0.0, 0.0, 0.0, 0.0, 0.0, 0.0, 0.0, 0.0, 0.0,
0.0, 0.0, 0.0, 0.0, 0.0, 0.0, 0.0, 0.0, 0.0, 0.0,
0.0, 0.0, 0.0, 0.0, 0.0, 0.0, 0.0, 0.0, 0.0, 0.0,
0.0, 0.0, 0.0, 0.0, 0.0, 0.0, 0.0, 0.0, 0.0, 0.0,
0.0, 0.0, 0.0, 0.0, 0.0, 0.0, 0.0, 0.0, 0.0, 0.0,
REDFRE, PHAA, PAXIS, PHAD, FORAMP,  PRAT,  RAMANG, MTYPE, MODINP  NSPC(S=5)
0.5884,     0.0, 0.652,    0.0,  0.03839,    1.0,        0.0,       0,        0,    3
REDFRE, FORAMP, for control surface
0.5884,        0.0,          0.038397243
```

START AEROELASTIC DATA, PHYLEN, DYNPRE, FREVEL
8.75, 1.10, 5165.
NMODES,NXMOD,NYMOD
6, 13, 13
XMOD
0.00000 0.08333 0.16667 0.25000 0.33333
0.41667 0.50000 0.58333 0.66667 0.75000
0.83333 0.91667 1.00000
YMOD
0.00000 0.07143 0.14286 0.21429 0.28571
0.35714 0.42857 0.50000 0.57143 0.64286
0.71429 0.78571 0.85714
MODE = 1
span station= 1
0.00000 0.00000 0.00000 0.00000 0.00000
0.00000 0.00000 0.00000 0.00000 0.00000
0.00000 0.00000 0.00000
span station= 2
0.00094 0.00138 0.00183 0.00231 0.00279
0.00328 0.00376 0.00428 0.00479 0.00542
0.00605 0.00660 0.00715
span station= 3
0.00188 0.00277 0.00366 0.00462 0.00558
0.00656 0.00753 0.00856 0.00958 0.01084
0.01209 0.01319 0.01429
span station= 4
0.00802 0.00995 0.01188 0.01384 0.01580
0.01779 0.01977 0.02186 0.02396 0.02625
0.02854 0.03071 0.03289
span station= 5
0.01416 0.01713 0.02010 0.02306 0.02602
0.02901 0.03200 0.03516 0.03833 0.04165
0.04498 0.04823 0.05148
span station= 6
0.03074 0.03451 0.03829 0.04203 0.04576
0.04953 0.05329 0.05717 0.06105 0.06503
0.06900 0.07297 0.07694
span station= 7
0.04732 0.05190 0.05649 0.06099 0.06550
0.07004 0.07457 0.07917 0.08377 0.08840
0.09303 0.09772 0.10240
span station= 8
0.07535 0.08005 0.08476 0.08941 0.09407

0.09875 0.10342 0.10813 0.11285 0.11759
0.12233 0.12712 0.13192
span station= 9
0.10338 0.10820 0.11303 0.11783 0.12264
0.12745 0.13227 0.13710 0.14193 0.14678
0.15163 0.15653 0.16144
span station= 10
0.14035 0.14473 0.14911 0.15349 0.15787
0.16226 0.16666 0.17107 0.17548 0.17991
0.18434 0.18882 0.19330
span station= 11
0.17733 0.18126 0.18519 0.18915 0.19310
0.19707 0.20105 0.20504 0.20903 0.21304
0.21705 0.22111 0.22516
span station= 12
0.22037 0.22349 0.22661 0.22975 0.23289
0.23605 0.23921 0.24238 0.24556 0.24875
0.25195 0.25516 0.25838
span station= 13
0.26341 0.26572 0.26804 0.27036 0.27269
0.27504 0.27738 0.27973 0.28209 0.28447
0.28684 0.28923 0.29161
MODE = 2
span station= 1
0.00000 0.00000 0.00000 0.00000 0.00000
0.00000 0.00000 0.00000 0.00000 0.00000
0.00000 0.00000 0.00000
span station= 2
0.01314 0.01547 0.01779 0.01830 0.01881
0.01799 0.01716 0.01526 0.01335 0.01040
0.00746 0.00295 -0.00156
span station= 3
0.02628 0.03093 0.03559 0.03660 0.03761
0.03597 0.03433 0.03051 0.02669 0.02081
0.01492 0.00590 -0.00312
span station= 4
0.07189 0.07579 0.07969 0.07839 0.07709
0.07165 0.06622 0.05722 0.04821 0.03585
0.02349 0.00737 -0.00874
span station= 5
0.11748 0.12064 0.12379 0.12017 0.11655
0.10733 0.09811 0.08392 0.06972 0.05089
0.03206 0.00884 -0.01437

span station= 6

0.16926 0.16524 0.16123 0.15130 0.14137
0.12621 0.11104 0.09112 0.07120 0.04708
0.02296 -0.00467 -0.03229

span station= 7

0.22103 0.20985 0.19867 0.18243 0.16619
0.14508 0.12398 0.09833 0.07267 0.04327
0.01386 -0.01817 -0.05021

span station= 8

0.22520 0.20788 0.19055 0.16941 0.14826
0.12332 0.09839 0.06996 0.04154 0.01031
-0.02091 -0.05407 -0.08722

span station= 9

0.22937 0.20590 0.18244 0.15638 0.13033
0.10156 0.07280 0.04160 0.01040 -0.02264
-0.05568 -0.08996 -0.12424

span station= 10

0.16305 0.13853 0.11402 0.08768 0.06135
0.03315 0.00496 -0.02484 -0.05465 -0.08564
-0.11664 -0.14848 -0.18031

span station= 11

0.09672 0.07116 0.04560 0.01899 -0.00763
-0.03525 -0.06287 -0.09129 -0.11970 -0.14865
-0.17760 -0.20699 -0.23639

span station= 12

-0.03402 -0.05564 -0.07726 -0.09950 -0.12175
-0.14453 -0.16730 -0.19045 -0.21360 -0.23703
-0.26045 -0.28407 -0.30767

span station= 13

-0.16479 -0.18246 -0.20014 -0.21801 -0.23588
-0.25382 -0.27175 -0.28963 -0.30751 -0.32542
-0.34332 -0.36115 -0.37897

MODE = 3

span station= 1

0.00000 0.00000 0.00000 0.00000 0.00000
0.00000 0.00000 0.00000 0.00000 0.00000
0.00000 0.00000 0.00000

span station= 2

-0.00679 -0.00707 -0.00735 -0.00602 -0.00468
-0.00171 0.00126 0.00597 0.01068 0.01811
0.02555 0.03740 0.04925

span station= 3

-0.01358 -0.01414 -0.01471 -0.01203 -0.00936

-0.00342 0.00251 0.01193 0.02135 0.03622
0.05109 0.07479 0.09849

span station= 4

-0.03150 -0.02936 -0.02721 -0.02002 -0.01283
-0.00015 0.01252 0.03131 0.05011 0.07671
0.10330 0.14097 0.17863

span station= 5

-0.04941 -0.04457 -0.03972 -0.02801 -0.01629
0.00311 0.02252 0.05069 0.07887 0.11719
0.15550 0.20713 0.25875

span station= 6

-0.06534 -0.05598 -0.04662 -0.03023 -0.01384
0.01038 0.03460 0.06719 0.09979 0.14123
0.18267 0.23478 0.28688

span station= 7

-0.08127 -0.06740 -0.05352 -0.03246 -0.01139
0.01765 0.04668 0.08369 0.12071 0.16528
0.20984 0.26243 0.31501

span station= 8

-0.09840 -0.08289 -0.06739 -0.04568 -0.02398
0.00423 0.03243 0.06692 0.10141 0.14165
0.18190 0.22784 0.27378

span station= 9

-0.11553 -0.09839 -0.08125 -0.05891 -0.03657
-0.00919 0.01818 0.05014 0.08211 0.11803
0.15395 0.19326 0.23255

span station= 10

-0.15643 -0.14017 -0.12392 -0.10399 -0.08406
-0.06061 -0.03716 -0.01055 0.01607 0.04534
0.07462 0.10606 0.13750

span station= 11

-0.19733 -0.18195 -0.16658 -0.14907 -0.13156
-0.11203 -0.09250 -0.07124 -0.04998 -0.02735
-0.00472 0.01887 0.04245

span station= 12

-0.26248 -0.24992 -0.23737 -0.22362 -0.20987
-0.19502 -0.18016 -0.16438 -0.14859 -0.13210
-0.11560 -0.09868 -0.08177

span station= 13

-0.32763 -0.31790 -0.30817 -0.29819 -0.28820
-0.27801 -0.26783 -0.25753 -0.24723 -0.23686
-0.22650 -0.21625 -0.20601

MODE = 4

span station= 1

0.00000	0.00000	0.00000	0.00000	0.00000
0.00000	0.00000	0.00000	0.00000	0.00000
0.00000	0.00000	0.00000		

span station= 2

-0.04823	-0.04818	-0.04813	-0.04264	-0.03716
-0.03076	-0.02436	-0.01895	-0.01353	-0.01137
-0.00921	-0.01177	-0.01433		

span station= 3

-0.09646	-0.09636	-0.09626	-0.08529	-0.07432
-0.06152	-0.04873	-0.03789	-0.02706	-0.02274
-0.01843	-0.02355	-0.02866		

span station= 4

-0.17605	-0.16102	-0.14598	-0.12421	-0.10244
-0.08129	-0.06015	-0.04528	-0.03042	-0.02700
-0.02357	-0.03362	-0.04367		

span station= 5

-0.25563	-0.22566	-0.19570	-0.16313	-0.13055
-0.10106	-0.07156	-0.05268	-0.03379	-0.03125
-0.02871	-0.04370	-0.05868		

span station= 6

-0.20796	-0.17015	-0.13234	-0.09996	-0.06759
-0.04361	-0.01963	-0.00921	0.00121	-0.00499
-0.01119	-0.03263	-0.05406		

span station= 7

-0.16029	-0.11463	-0.06897	-0.03680	-0.00463
0.01384	0.03230	0.03425	0.03620	0.02127
0.00634	-0.02156	-0.04944		

span station= 8

-0.00518	0.02252	0.05022	0.06556	0.08090
0.08343	0.08595	0.07430	0.06265	0.03770
0.01276	-0.02154	-0.05583		

span station= 9

0.14992	0.15966	0.16941	0.16792	0.16643
0.15302	0.13961	0.11435	0.08909	0.05414
0.01918	-0.02152	-0.06221		

span station= 10

0.20459	0.19641	0.18824	0.17205	0.15587
0.13124	0.10661	0.07394	0.04128	0.00240
-0.03647	-0.07886	-0.12124		

span station= 11

0.25925	0.23316	0.20706	0.17619	0.14531
0.10946	0.07361	0.03354	-0.00654	-0.04933

-0.09212 -0.13619 -0.18026

span station= 12

0.10471 0.07608 0.04743 0.01603 -0.01537
-0.04942 -0.08347 -0.11952 -0.15558 -0.19278
-0.22999 -0.26754 -0.30508

span station= 13

-0.04984 -0.08103 -0.11222 -0.14414 -0.17607
-0.20832 -0.24057 -0.27261 -0.30464 -0.33626
-0.36788 -0.39890 -0.42992

MODE = 5

span station= 1

0.00000 0.00000 0.00000 0.00000 0.00000
0.00000 0.00000 0.00000 0.00000 0.00000
0.00000 0.00000 0.00000

span station= 2

-0.03536 -0.03097 -0.02658 -0.01511 -0.00364
0.01008 0.02381 0.03417 0.04453 0.04754
0.05056 0.04713 0.04371

span station= 3

-0.07072 -0.06193 -0.05315 -0.03022 -0.00729
0.02017 0.04762 0.06834 0.08905 0.09509
0.10112 0.09427 0.08741

span station= 4

-0.11931 -0.09409 -0.06887 -0.03081 0.00726
0.04649 0.08572 0.11031 0.13489 0.13444
0.13400 0.11281 0.09162

span station= 5

-0.16790 -0.12625 -0.08460 -0.03140 0.02180
0.07281 0.12382 0.15227 0.18072 0.17379
0.16687 0.13134 0.09582

span station= 6

-0.15491 -0.11006 -0.06520 -0.01797 0.02927
0.06636 0.10344 0.11448 0.12552 0.10259
0.07965 0.02932 -0.02101

span station= 7

-0.14193 -0.09387 -0.04581 -0.00454 0.03674
0.05990 0.08307 0.07669 0.07031 0.03138
-0.00756 -0.07271 -0.13785

span station= 8

-0.11041 -0.07607 -0.04172 -0.01766 0.00641
0.01258 0.01874 0.00031 -0.01813 -0.06166
-0.10518 -0.16907 -0.23296

span station= 9

-0.07890 -0.05827 -0.03764 -0.03077 -0.02391
-0.03474 -0.04558 -0.07607 -0.10657 -0.15469
-0.20280 -0.26544 -0.32807
span station= 10
-0.02216 -0.01178 -0.00140 -0.00233 -0.00325
-0.01757 -0.03189 -0.06030 -0.08871 -0.12948
-0.17025 -0.22104 -0.27183
span station= 11
0.03458 0.03471 0.03483 0.02612 0.01740
-0.00040 -0.01819 -0.04452 -0.07085 -0.10427
-0.13769 -0.17664 -0.21559
span station= 12
0.18799 0.18414 0.18029 0.17089 0.16149
0.14645 0.13140 0.11124 0.09108 0.06671
0.04234 0.01488 -0.01258
span station= 13
0.34143 0.33359 0.32576 0.31568 0.30560
0.29331 0.28102 0.26703 0.25303 0.23771
0.22239 0.20642 0.19046
MODE = 6
span station= 1
0.00000 0.00000 0.00000 0.00000 0.00000
0.00000 0.00000 0.00000 0.00000 0.00000
0.00000 0.00000 0.00000
span station= 2
-0.03769 -0.02884 -0.01999 -0.00234 0.01532
0.03021 0.04509 0.04324 0.04140 0.01334
-0.01472 -0.07554 -0.13636
span station= 3
-0.07538 -0.05768 -0.03999 -0.00467 0.03065
0.06042 0.09018 0.08649 0.08279 0.02667
-0.02945 -0.15109 -0.27272
span station= 4
-0.12189 -0.08267 -0.04345 0.01008 0.06361
0.10166 0.13969 0.12469 0.10968 0.02425
-0.06118 -0.21331 -0.36542
span station= 5
-0.16840 -0.10766 -0.04691 0.02483 0.09657
0.14289 0.18920 0.16288 0.13656 0.02182
-0.09291 -0.27552 -0.45811
span station= 6
-0.16755 -0.10425 -0.04094 0.02437 0.08968
0.12684 0.16400 0.14070 0.11739 0.02969

-0.05802 -0.18405 -0.31008

span station= 7

-0.16670 -0.10084 -0.03497 0.02391 0.08279
0.11079 0.13879 0.11851 0.09822 0.03755
-0.02312 -0.09259 -0.16205

span station= 8

-0.18162 -0.12498 -0.06833 -0.01746 0.03341
0.06403 0.09465 0.09589 0.09713 0.07596
0.05479 0.03330 0.01181

span station= 9

-0.19653 -0.14912 -0.10169 -0.05883 -0.01597
0.01727 0.05050 0.07327 0.09604 0.11437
0.13270 0.15919 0.18567

span station= 10

-0.22110 -0.17930 -0.13750 -0.09761 -0.05772
-0.02191 0.01390 0.04609 0.07829 0.11091
0.14352 0.18372 0.22392

span station= 11

-0.24566 -0.20948 -0.17330 -0.13639 -0.09948
-0.06109 -0.02271 0.01891 0.06054 0.10744
0.15433 0.20826 0.26218

span station= 12

-0.25895 -0.22990 -0.20085 -0.17022 -0.13959
-0.10632 -0.07305 -0.03585 0.00136 0.04356
0.08576 0.13295 0.18013

span station= 13

-0.27223 -0.25031 -0.22840 -0.20405 -0.17970
-0.15155 -0.12341 -0.09062 -0.05782 -0.02032
0.01718 0.05762 0.09806

Generalized Mass Matrix

0.36051E-05	0.	0.	0.	0.	0.
0.	0.45913E-05	0.	0.	0.	0.
0.	0.	0.47239E-05	0.	0.	0.
0.	0.	0.	0.48252E-05	0.	0.
0.	0.	0.	0.	0.50495E-05	0.
0.	0.	0.	0.	0.	0.73964E-05

DAMPING

0.000,	0.000,	0.000,	0.000,	0.000,	0.000
0.000,	0.000,	0.000,	0.000,	0.000,	0.000
0.000,	0.000,	0.000,	0.000,	0.000,	0.000
0.000,	0.000,	0.000,	0.000,	0.000,	0.000
0.000,	0.000,	0.000,	0.000,	0.000,	0.000
0.000,	0.000,	0.000,	0.000,	0.000,	0.000

Generalized Stiffness Matrix

0.68240E-01	0.	0.	0.	0.	0.
0.	0.12852E+01	0.	0.	0.	0.
0.	0.	0.28045E+01	0.	0.	0.
0.	0.	0.	0.10453E+02	0.	0.
0.	0.	0.	0.	0.19442E+02	0.
0.	0.	0.	0.	0.	0.46899E+02

GEN DIS
0.2, 0.2, 0.0, 0.0, 0.0, 0.0
GEN VEL
0.0, 0.0, 0.0, 0.0, 0.0, 0.0
GEN ACC
0.0, 0.0, 0.0, 0.0, 0.0, 0.0

REPORT DOCUMENTATION PAGE

Form Approved
OMB No. 0704-0188

1. AGENCY USE ONLY *(Leave blank)*	2. REPORT DATE	3. REPORT TYPE AND DATES COVERED
	October 1994	Technical Memorandum

4. TITLE AND SUBTITLE
User's Guide for ENSAERO–A Multidisciplinary Program for Fluid/ Structural/Control Interaction Studies of Aircraft (Release 1)

5. FUNDING NUMBERS
509-10-11

6. AUTHOR(S)
Guru P. Guruswamy

7. PERFORMING ORGANIZATION NAME(S) AND ADDRESS(ES)
Ames Research Center
Moffett Field, CA 94035-1000

8. PERFORMING ORGANIZATION REPORT NUMBER
A-94148

9. SPONSORING/MONITORING AGENCY NAME(S) AND ADDRESS(ES)
National Aeronautics and Space Administration
Washington, DC 20546-0001

10. SPONSORING/MONITORING AGENCY REPORT NUMBER
NASA TM-108853

11. SUPPLEMENTARY NOTES
Point of Contact: Guru P. Guruswamy, Ames Research Center, MS 258-1,
Moffett Field, CA 94035-1000; (415) 604-6329

12a. DISTRIBUTION/AVAILABILITY STATEMENT
Unclassified-Unlimited
Subject Category – 01

12b. DISTRIBUTION CODE

13. ABSTRACT ***(Maximum 200 words)***

Strong interactions can occur between the flow about an aerospace vehicle and its structural components resulting in several important aeroelastic phenomena. These aeroelastic phenomena can significantly influence the performance of the vehicle. At present, closed-form solutions are available for aeroelastic computations when flows are in either the linear subsonic or supersonic range. However, for aeroelasticity involving complex nonlinear flows with shock waves, vortices, flow separations, and aerodynamic heating, computational methods are still under development. These complex aeroelastic interactions can be dangerous and limit the performance of aircraft. Examples of these detrimental effects are aircraft with highly swept wings experiencing vortex-induced aeroelastic oscillations, transonic regime at which the flutter speed is low, aerothermoelastic loads that play a critical role in the design of high-speed vehicles, and flow separations that often lead to buffeting with undesirable structural oscillations. The simulation of these complex aeroelastic phenomena requires an integrated analysis of fluids and structures. This report presents a summary of the development, applications, and procedures to use the multidisciplinary computer code ENSAERO. This code is based on the Euler/ Navier–Stokes flow equations and modal/finite-element structural equations.

14. SUBJECT TERMS
Euler/Navier–Stokes, Unsteady, Aerodynamics, Aeroelasticity

15. NUMBER OF PAGES
48

16. PRICE CODE
A03

17. SECURITY CLASSIFICATION OF REPORT	18. SECURITY CLASSIFICATION OF THIS PAGE	19. SECURITY CLASSIFICATION OF ABSTRACT	20. LIMITATION OF ABSTRACT
Unclassified	Unclassified		